AAPM REPORT NO. 246

Estimating Patient Organ Dose with Computed Tomography: A Review of Present Methodology and Required DICOM Information

A Joint Report of AAPM Task Group 246 and the European Federation of Organizations for Medical Physics (EFOMP)

August 2019

This page intentionally left blank.

Estimating Patient Organ Dose with Computed Tomography: A Review of Present Methodology and Required DICOM Information

A Joint Report of AAPM Task Group 246 and the European Federation of Organizations for Medical Physics (EFOMP)

Jonas Andersson, Chair[1], William Pavlicek, Co-Chair[2], Rani Al-Senan[3], Wesley Bolch[4], Hilde Bosmans[5], Dianna Cody[6], Robert Dixon[7], Paola Colombo[8], Frank Dong[9], Sue Edyvean[10], Jan Jansen[10], Kalpana Kanal[11], Shuai Leng[12], Qing Liang[13], Cynthia McCollough[12], Ed McDonagh[14], Michael McNitt-Gray[15], Robert Paden[2], Madan Rehani[16], Ehsan Samei[17], Ioannis Sechopoulos[18], Mark Supanich[19], Christine Theodorakou[20], Xiaoyu Tian[17], Alberto Torresin[21], Annalisa Trianni[22], David Zamora[11], and Federica Zanca[23]

[1]Umeå University, Umeå, SE
[2]Mayo Clinic, Phoenix, AZ, USA
[3]Columbia University, New York, NY, USA
[4]University of Florida, Gainesville, FL, USA
[5]University of Leuven, Leuven, BE
[6]MD Anderson Cancer Hospital, Houston, TX, USA
[7]Wake Forest University School of Medicine, NC, USA
[8]Niguarda Ca'Granda Hospital, Milano, IT
[9]Cleveland Clinic, Cleveland, OH, USA
[10]Computing Center, HPA, Oxfordshire, UK
[11]University of Washington Medical Center, WA, USA
[12]Mayo Clinic, Rochester, MN, USA
[13]Mercy Health System, Janesville, WI, USA
[14]Royal Marsden Hospital, London, UK
[15]David Geffen School of Medicine, UCLA, CA, USA
[16]European Society of Radiology, Vienna, AU
[17]Duke University, Durham, NC, USA
[18]Radboud University Medical Center, Nijmegen, NL
[19]Rush Presbyterian Hospital, Chicago, IL, USA
[20]Christie Medical Physics, Wilmslow, Manchester, UK
[21]Niguarda Ca' Granda Hospital, Milano, IT
[22]AZ University Hospital, Udine, IT
[23]GE Healthcare, Paris, FR

Task Group Consultants

Erin Angel	Canon Medical Systems, USA
Nicholas Bevins	Henry Ford Medical Systems, Detroit, MI, USA
Kevin Buckley	Boston Children's Hospital, Boston, MA, USA
Gregory Couch	Radimetrics, Toronto, CA
Thaddeus Flood	Director, MITA, Washington, DC, USA
Dustin Gress	MD Anderson Cancer Hospital, Houston, TX, USA
Sofia Kottou	University of Athens, Athens, GR
Mary Sue Kulpins	GE Healthcare, USA
Richard Morin	Mayo Clinic, Jacksonville, FL, USA
William O'Connell	GE Healthcare, USA
Renato Padovani	University Hospital, Undine, IT
Anthony Seibert	University of California, Davis Medical Center, Irvine, CA, USA
Stanley Stern	FDA, USA
Orhan Suleiman	FDA, USA (ret)
Makoto Suzuki	Japan Medical Imaging and Radiological Systems Industries Association, JP
Virginia Tsapaki	Konstantopoulio General Hospital, Athens, GR
Stephen Vastagh	General Secretary, DICOM, USA

DISCLAIMER: This publication is based on sources and information believed to be reliable, but the AAPM, the authors, and the publisher disclaim any warranty or liability based on or relating to the contents of this publication.

The AAPM does not endorse any products, manufacturers, or suppliers. Nothing in this publication should be interpreted as implying such endorsement.

ISBN: 978-1-936366-72-9
ISSN: 0271-7344

Published by

American Association of Physicists in Medicine
1631 Prince Street
Alexandria, VA 22314

Contents

1. Introduction 7
1.1 Purpose and Overview 7
1.2 Out of Scope 7
2. Current Dosimetry Metrics and Associated DICOM Information 8
2.1 Overview of the CTDI and its Derivatives 8
2.1.1 $CTDI_{100}$, $CTDI_{w}$, $CTDI_{vol}$ and $CTDI_{free\text{-}in\text{-}air}$ 8
2.1.2 Tolerance Levels 9
2.1.3 Special Considerations for Nominal Beam Collimations >40 mm 10
2.1.4 $CTDI_{vol}$ for Examination Protocols Without Table Translation 11
2.2 Wide Beam Dosimetry and Equilibrium Dose: AAPM Report 111 11
2.3 The Dose Length Product (DLP) 12
2.4 The CT Localizer Radiograph 12
2.5 Scanner Parameters Connected to $CTDI_{vol}$ and DLP in DICOM Image Header Tags 13
2.6 Size-Specific Dose Estimates (SSDE) and Water-Equivalent Diameter (WED) 14
2.6.1 SSDE and Longitudinal Variations in Patient Dimension 14
2.6.2 Calculation of WED 15
3. Current and Emerging Methods to Estimate Organ Dose 15
3.1 Studies on the Accuracy and Utility of SSDE in Estimating Organ Doses 16
3.1.1 Typical Head and Body Examinations (Contiguous Axial and Helical) 16
3.1.2 Perfusion Examinations 18
3.2 Organ Dose Estimates with Regional $CTDI_{vol}$ Values 19
3.3 Application of the Convolution Method for Organ Dose Estimation 19
3.4 Monte Carlo Simulation Methods 22
3.4.1 Monte Carlo Engines and Computational Phantoms 22
3.4.2 Modeling of the X-ray Source 23
3.4.3 Monte Carlo and Normalization of Reported Organ Dose 24
3.4.4 Generic Axial Dose Libraries vs. Helical Protocol-Specific Dose Libraries 24
3.4.5 Considerations of Starting Angle and Overranging 24
3.4.6 Monte Carlo and Modeling of TCM 24
3.5 Monte Carlo Simulation with Stylized Anthropomorphic Phantoms 25
3.6 Monte Carlo Simulation to Model the Dose Deposited by a CT Scanner 26
3.7 Benchmarking and Validation of Monte Carlo Simulations 27
4. Sources of Uncertainty in Estimating Organ Dose 27
4.1 Uncertainties in SSDE–based Calculations of Patient Organ Dose 28
4.1.1 Pencil Ionization Chamber Measurements and $CTDI_{vol}$ 28
4.1.2 The SSDE 28
4.1.3 SSDE and TCM Examinations 29
4.1.4 Patient Not Centered in the Gantry 29
4.1.5 The SSDE and Partial Organ Irradiation 29
4.2 Uncertainties in Monte Carlo Estimates of Organ Dose 29
4.2.1 Computational Phantoms 29
4.2.2 Scanner Irradiation Conditions 30
4.2.3 Patient Not Centered in the Gantry 30
4.3 Contrast Media Used in CT Examinations 31
4.4 Reporting Uncertainty with Estimates of Patient Organ Dose 31
5. Summary of Report and Recommendations 31
6. References 33
Appendix: DICOM—Present and Future for Dosimetry and Estimating Organ Dose . . . 40

1. Introduction

The radiation absorbed dose or 'dose' that a patient receives from a routine CT examination is considered to yield very low risk of harm when properly used to obtain a diagnostic benefit, i.e., when the justification and optimization of a given examination have been taken into account.[1] However, a gap is recognized in the ability of the conventional CT radiation dosimetry metrics—the Computed Tomography Dose Index (CTDI) and Dose Length Product (DLP)[2]—to accurately represent individual patient organ doses. Organ dose is generally regarded as one of the best metrics to quantify individual radiation burden.

1.1 Purpose and Overview

The purpose of this report is (1) to summarize the current state of the art in estimating organ doses from CT examinations and (2) to outline a road map for standardized reporting of essential parameters necessary for estimation of organ doses from CT imaging in the DICOM standard. To address these purposes, the report includes a comprehensive discussion of (1) the various metrics, concepts, and methods that may be used to achieve estimates of patient organ dose and (2) the DICOM standard for CT.

This Joint Report of the American Association of Physicists in Medicine (AAPM) Task Group 246 and the European Federation of Organizations for Medical Physics (EFOMP) contains three major sections and an appendix. Section 2 (with additional material in the appendix) provides a review of basic CT dosimetry metrics, their uses and limitations in the context of organ dosimetry, and the DICOM information currently associated with parameters that affect CT dose metrics and, consequently, organ dose estimates. Section 3 provides an overview of present and emerging organ dose estimation methods reported in the literature, e.g., for the lens of the eye, breast tissue, colon, and skin. Finally, the report concludes with section 4, which provides a discussion on the sources and magnitudes of uncertainty for different organ dose estimation methods.

Ongoing efforts to facilitate routine standardized estimation of patient organ doses from CT are dependent, in large part, on the availability of the DICOM Radiation Dose Structured Report (RDSR), which provides a host of information pertinent to radiation dose calculations. This report, therefore, includes detailed information on DICOM header content in CT images and how it can be used in organ dose estimation. The RDSR markedly expands the abilities of the clinical medical physicist to estimate doses at the patient, device, and protocol level.[3,4]

1.2 Out of Scope

Effective dose, while important from a general radiation protection viewpoint, is not addressed in this report. This quantity is used to account for partial body exposures to ionizing radiation and to reflect the associated radiation detriment for populations of workers and the general public. This quantity provides an estimate of detriment by weighting the absorbed dose to organs and tissues according to the sensitivity of the exposed tissues and organs to ionizing radiation, as well as according to the quality, or linear energy transfer, or the applied type of radiation.[4] Macroscopic irradiation conditions are commonly used to determine the effective dose, e.g., the DLP for CT examinations, which means that characteristics of a specific individual that will influence organ dose and radiation detriment are not taken into account. Effective dose is commonly used to compare doses delivered by different exposure conditions, such as to compare the radiation detriment from medical imaging to that from the dose received from naturally occurring background sources of radiation. Such comparisons are helpful in discussing the relative risk and justification of a given examination. Present methodology for estimating individual patient organ dose is the subject of this report, and thus the effective dose concept is out of scope.

2. Current Dosimetry Metrics and Associated DICOM Information

2.1 Overview of the CTDI and its Derivatives

The computed tomography dose index (CTDI) is a quantity developed to reflect the amount of radiation produced by a CT scan in a standardized fashion.[5,6] It is determined from a measurement of the scanner's radiation output using a single rotation of the x-ray source with a static table. The CTDI metric is given in units of gray (Gy), usually mGy, i.e., absorbed dose or energy deposited per unit mass (i.e., J/kg). CTDI and its derivatives are described in detail elsewhere, and only briefly reviewed here.[7–10]

2.1.1 $CTDI_{100}$, $CTDI_{w}$, $CTDI_{vol}$ and $CTDI_{free\text{-}in\text{-}air}$

CTDI is formally defined[2] as

$$CTDI_{\infty} = \frac{1}{NT}\int_{-\infty}^{\infty} D(z)dz. \tag{1}$$

Depending on the calibration of the dosimetry system used, air kerma, $K(z)$, may be directly measured instead of absorbed dose, $D(z)$, in the patient longitudinal direction, or z-axis. While the CTDI can be correctly defined in either term (absorbed dose or air kerma), we shall use absorbed dose in this report. The CTDI is defined using an infinite integral of the dose profile, $D(z)$, along the z-axis. To produce the CTDI, the dose integral is divided by the nominal beam collimation, $\Delta d = NT$. The nominal collimation is the product of the number of physical data channels, N, and the width of one detector data channel in the z-axis, T. It is important to note that the reconstructed image thickness and the detector data channel width are commonly described by the same term, 'slice' (as in a 64-slice CT scanner or a 3-mm image slice). In this report, the term 'slice' only refers to the number of data channels N, each of width T.

As measurements cannot be performed using infinity as integration limits, the conventional application of the CTDI formalism involves performing measurements using a calibrated 100-mm-long pencil ionization chamber and an electrometer,[5,11]

$$CTDI_{100} = \frac{1}{NT}\int_{-50\text{ mm}}^{50\text{ mm}} D(z)dz, \tag{2}$$

where the pencil ionization chamber reading represents a direct measurement of the integral in Equation (2). The physical interpretation of the $CTDI_{100}$ is the dose at the center of a 100-mm scan length for a table increment per rotation $\Delta d = NT$.[6] $CTDI_{\infty}$ (described further in section 2.2) is the asymptotic (equilibrium) dose reached at the central slice of a large scan length.[12]

The $CTDI_{100}$ alternatively can be determined empirically by measuring the spatial distribution of absorbed dose, $D(z)$, along the z-axis in a CTDI phantom. This approach requires a dosimeter capable of performing measurements with a high spatial resolution, e.g., a small-measurement-volume ionization chamber or a solid-state detector. An example of the dose profile acquired using a small-volume detector is given in Figure 1 for a nominal collimation of 5 mm. Because the pencil ionization chamber is 10 cm long, the scattered radiation tails of the dose profile are not fully captured. Due to this truncation, the measured $CTDI_{100}$ underestimates $CTDI_{\infty}$ (i.e., equilibrium dose, as discussed below) by approximately 20% for nominal beam collimations of ≤40 mm.[2] Wider nominal beam collimations cause more extensive underrepresentation of the equilibrium dose by $CTDI_{100}$.[2,13] In spite of this underestimation of the equilibrium dose, $CTDI_{100}$ is a robust, standardized measurement of the radiation output for purposes of annual and post-maintenance CT quality control (see section 2.1.2).

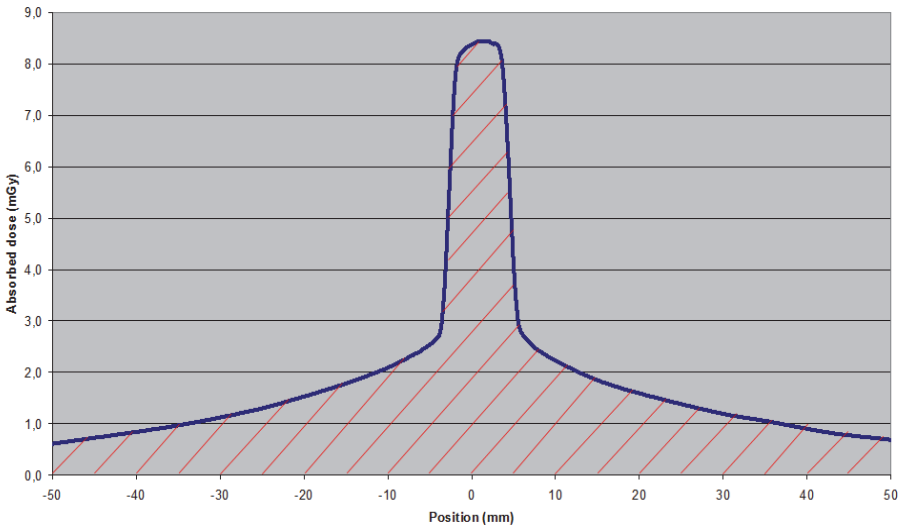

Figure 1. Example of a dose profile from a CT scan acquired with a nominal collimation of 5 mm. The dose profile was measured along the central axis of a CTDI head phantom (16 cm diameter) with a liquid ionization chamber calibrated for dose to water.[14,15]

The weighted CTDI, $CTDI_w$, is the $CTDI_{100}$ calculated from measurements made at the center and periphery of standardized phantoms of a specified size and composition, which represent a simplified "head" and "body" patient cross section. The head CTDI phantom is 16 cm in diameter, and the body CTDI phantom is 32 cm in diameter. Both are made of polymethylmethacrylate, PMMA, e.g., acrylic, (r = 1.19 ±0.01 g cm^{-3}). The 'w' refers to a weighting of the measurements made at the edge and periphery of the CTDI measurement phantom (1/3 of the center value and 2/3 of the periphery value). $CTDI_w$ represents the average dose over the central plane of a 100-mm scan length.

The volume CTDI, $CTDI_{vol}$, takes into account any overlaps or gaps between successive rotations of the x-ray tube. For contiguous source rotations (table travel per rotation = nominal beam collimation), $CTDI_w = CTDI_{vol}$. For noncontiguous source rotations,

$$CTDI_{vol} = \frac{NT}{\Delta d} CTDI_w , \tag{3}$$

$CTDI_w$ is divided by the pitch value (in helical scanning) or the table increment divided by the nominal beam collimation (in axial scanning).

The $CTDI_{free\text{-}in\text{-}air}$ is based on the same concept as the CTDI measured in a phantom, but the $CTDI_{free\text{-}in\text{-}air}$ is measured in air, usually at isocenter, as opposed to at locations within the field of view that correspond to standard positions within the CTDI phantom. This metric is often used for quantifying the x-ray output from the scanner. Because it can be measured without the use of CTDI phantoms, it can be easily used for quality assurance purposes. $CTDI_{free\text{-}in\text{-}air}$ is also required for certain Monte Carlo dose estimation data sets, for example those from the National Radiological Protection Board.[16,17]

2.1.2 Tolerance Levels

A part of the uncertainty in organ dose estimates comes from uncertainties in the reported $CTDI_{vol}$, which is used in several present and emerging dosimetry methods, and derived from measured $CTDI_w$

Table 1: Examples of typical tolerance levels for the $CTDI_w$ according to five different CT manufacturers (A–E)

Manufacturer	X-ray Tube Potential (kV)	Typical or Expected $CTDI_w$ Tolerance	Maximum Tolerance
A	kV < 80 kV > 80	±15% ±15%	±40% ±30%
B		±15%	±40%
C	80–140 kV Narrow collimation (2×0.625 mm, 2×0.5 mm)		±25% ±30%
D	120 kV		±20%
E	80–140 kV	±20%	±20%

values. $CTDI_w$ tolerance levels are determined by manufacturers and reported to regulatory agencies at the time that they submit for product market clearance. They correspond to the allowable differences between measured and displayed $CTDI_{vol}$ values for contiguous scans, and they often vary between different manufacturers and modes of scanner operation, e.g., x-ray tube potential and nominal collimation. Differences that fall within these tolerances are not considered by the manufacturer to require any service action. In Table 1, examples of typical tolerance levels as determined by five different CT manufacturers are given (personal communication, Medical Imaging and Technology Alliance (MITA)).

From a dosimetry perspective, CT scanners typically demonstrate a high degree of reproducibility between different makes and models,[18] with relative reproducibility errors under 5%, well below the $CTDI_w$ tolerances stated by the manufacturers in Table 1. However, many factors may influence the $CTDI_w$ values for individual scanners: age of x-ray tube, calibration of scanner, dosimetry system used and its calibration, measurement setup, and technical parameters such as x-ray tube potential (especially lower tube potential settings as described for manufacturer A in Table 1), tube current (mA), and the nominal collimation. The tolerances are typically higher for narrow collimations (e.g., manufacturer C in Table 1) due to uncertainty in actual beam width and higher dose contributions from beyond the imaged volume, i.e., penumbra.[19]

Medical physicists commonly compare their CTDI measurements to the manufacturer-reported $CTDI_{vol}$, which is based on the manufacturer-determined $CTDI_w$. The $CTDI_{vol}$, which is displayed on the operator console, represents an average value of $CTDI_w$ values measured on many systems of the same model and software version. Each manufacturer's operation manual specifies the tolerance values for differences between their average $CTDI_w$ values and those measured by the user. The measurement precision achieved by an individual user on a specific scanner is typically much smaller than the tolerances specified by the manufacturer.[18]

2.1.3 Special Considerations for Nominal Beam Collimations >40 mm

Due to the availability of CT scanners with relatively wide nominal collimation values, the IEC has adopted a modified definition[2] of the $CTDI_{100}$ for nominal beam collimations >40 mm, as described by

$$CTDI_{100} = \frac{1}{(NT)_{REF}} \int D_{REF}(z)\, dz \cdot \frac{CTDI_{NT}^{free\text{-}in\text{-}air}}{CTDI_{REF}^{free\text{-}in\text{-}air}}. \quad (4)$$

Here, parameters with a subscript *REF* should be evaluated in a standard CTDI phantom and with a value of $(NT)_{REF} \leq 20$ mm.

The $CTDI_{free\text{-}in\text{-}air}$ can be measured by using either an ionization chamber with a small measurement volume, such as the liquid ionization chamber, or a solid-state detector.[14,15] The dosimeter is translated (stepped) through the x-ray beam using either the patient table or a separate stepping motor system to measure the entire dose profile. $CTDI_{free\text{-}in\text{-}air}$ can also be measured with pencil ionization chambers having a length suitable for a given nominal collimation. The modified $CTDI_{100}$ values are used to calculate the $CTDI_w$ and $CTDI_{vol}$, as previously described. An in-depth discussion on the introduction and justification of Equation (4) for interested readers is found in IEC 60601-2-44 Edition 3.2.[2]

A recent International Atomic Energy Agency (IAEA) report on the status of computed tomography dosimetry for wide cone-beam CT scanners provides practical advice on measuring $CTDI_{free\text{-}in\text{-}air}$ without recourse to special chambers and using the standard-length (100 mm) pencil ionization chamber.[20] The Institute of Physics and Engineering in Medicine (IPEM) also provides practical advice on implementing this approach.[21]

2.1.4 $CTDI_{vol}$ for Examination Protocols Without Table Translation

Scanner-reported $CTDI_{vol}$ values significantly overestimate the actual dose to the patient when there is no table translation. This is because the reported $CTDI_{vol}$ is based on the $CTDI_{100}$, i.e., reflecting a scan length and scatter volume of 100 mm, where the tails of each individual dose profile are integrated to represent the average dose in the center of the scan volume resulting from multiple contiguous rotations of the x-ray source. This is not equivalent to the average dose in the center of the scan for a single, axial rotation of a narrow beam, where scatter tails from adjacent rotations of the source are not additive to the dose in the center of the scan volume. This effect becomes more pronounced at narrower beam collimations ($NT < 20$ mm).[2] The resulting $CTDI_{vol}$ value overestimates the peak dose to the irradiated tissue by as much as 300% for certain perfusion studies and bolus tracking scans.[22,23]

The difference between the CT scanner-reported $CTDI_{vol}$ and the peak skin dose within the scan volume for scans without table translation can be estimated by dividing the peripheral $CTDI_{100}$ by the peak peripheral dose for a standard CTDI phantom, which can be determined using a small 0.6 cm^3 Farmer-type chamber centered in the scan volume, or direct measurement of the radiation dose profile.[23] As an example, measurements on a GE LightSpeed VCT scanner with a beam width setting of 10 mm (120 kV) yielded a $CTDI_{100}$ of 21.3 mGy and peak peripheral dose of 7.5 mGy for 100 mAs, corresponding to an overestimation of 284% (personal communication; Jonas Andersson, Umeå University, Sweden).

2.2 Wide Beam Dosimetry and Equilibrium Dose: AAPM Report 111

A comprehensive methodology for the evaluation of radiation dose in CT applications is given in AAPM Report 111.[12] The report presents a measurement paradigm that can be applied to any scan mode (axial or helical), fan- or cone-beam scanners, and to stationary scans or those that perform translation of the table during scanning. A small-volume ionization chamber (e.g., 0.6 cm^3 Farmer-type chamber) and a long CTDI phantom (e.g., 300 mm) are used to measure the accumulated dose distributions for different measurement lengths, *L*.

With increasing *L*, the cumulative dose increases due to additional contributions from the radiation scatter tails of the dose profile. Eventually, the cumulative dose reaches an equilibrium dose, i.e., the contribution of the dose profile tails will eventually (for large values of *L*) be negligible. This upper limiting value is called the *equilibrium dose*,[12] and it is determined by an infinite integral of the dose profile over the patient table translation that occurs for a particular scan. The equilibrium dose for a table increment of $\Delta d = NT$ (a pitch of unity) is given by $CTDI_\infty$ in Equation (1).

The AAPM Task Group 200 report, *CT Dosimetry Phantoms and the Implementation of AAPM Report Number 111*, describes a practical method for measuring the equilibrium dose that should address some of the limitations of CTDI metrics.[24]

2.3 The Dose Length Product (DLP)

Using the CTDI formalism, an estimate of the integrated absorbed dose to a scanned volume of tissue having a length L is given by the dose length product (DLP), which is defined for axial, Equation (5), and helical scans, Equation (6), respectively, as

$$DLP_{axial} = CTDI_{vol} \cdot \Delta d \cdot n, \tag{5}$$

$$DLP_{helical} = CTDI_{vol} \cdot L. \tag{6}$$

Here, L represents the total table travel distance (cm) during the irradiation event, n is the number of rotations in an axial scan, and Δd the table translation per rotation. It is important to note that for helical scanning, L typically exceeds the scan range prescribed by the user in order to acquire needed projection data beyond the limits of the image reconstruction range, a concept referred to as over-ranging. Again, L represents the length over which radiation was delivered, which is not necessarily equal to the length over which images can be produced. Scanner calculations of DLP take this over-ranging of the beam into account as the scanner knows the precise length of the irradiation event, a number that is not reported to the user.

When a user calculates the DLP according to Equations (5) or (6), care must be taken, therefore, to take over-ranging into account, as otherwise the user-calculated results may differ substantially from those reported in the Dose Data Page or RDSR.

To reduce the extra radiation applied during over-ranging, multiple manufacturers have implemented beam collimators that can be quickly opened and closed at the beginning and ending of the scan, respectively, to greatly reduce the unwanted over-ranging radiation.[25] Here also, the true irradiation length is not reported to the user. However, as the adaptive collimators block the majority of the additional radiation that is applied due to over-ranging, the agreement between the user-calculated and the scanner-calculated values of DLP will be much better.

2.4 The CT Localizer Radiograph

The CTDI formalism was developed specifically for CT, where an x-ray source rotates around the patient. However, manufacturers have applied this concept to irradiation with a fixed source position, based on the premise that the x-ray beam undergoes the same attenuation by the cylindrically symmetric CTDI phantom whether or not the gantry is rotating. The "localizer $CTDI_{vol}$" is then calculated from the $CTDI_w$ per tube load Q determined in the standard fashion from a rotating gantry, where Q is the tube-current-time product (tube current × rotation time, i.e., mAs or total charge) used to produce x-rays during the rotation. Using the ratio $CTDI_w/Q$ determined at the same tube potential and beam collimation NT used for the localizer,

$$CTDI_{vol}^{localizer} = \frac{CTDI_W}{Q} \cdot I \cdot \frac{NT}{v}, \tag{7}$$

where I is the CT localizer tube current and v the table velocity (mm s^{-1}), DICOM tag (0018,9309). However, special consideration is required if the $CTDI_{vol}^{localizer}$ is used to estimate patient organ dose since the absorbed dose to individual organs from a planar projection is not accurately represented by the spatially averaged dose in a CTDI phantom.

It is important to note that the use of $CTDI_{vol}$ in this manner has not been vetted nor endorsed by the peer-review process, but was rather adopted by the manufacturers without support of the scientific

community. In order to accurately estimate organ or skin doses from a CT localizer radiograph, the attenuation of the planar projection radiograph by the patient must be adequately accounted for, just as one would do for standard radiography exposures. The manufacturers' approach of using $CTDI_{vol}$ to report doses from the CT localizer radiograph does not do this and is, in the opinion of AAPM Task Group 246 and EFOMP, not a sound dosimetric approach. Thus, we recommend against using $CTDI_{vol}$ in this manner. In particular, the $CTDI_{vol}$ associated with a CT localizer radiography should NOT be used to estimate patient dose.

2.5 Scanner Parameters Connected to $CTDI_{vol}$ and DLP in DICOM Image Header Tags

Many different physical scanner parameters must be taken into account when determining CTDI-based metrics. Examples of such scanner parameters that are stored in various DICOM image header tags are shown in Table 2.[26]

Table 2: Sample values for DICOM image header tags and a CT head examination[26]

DICOM Tag	Sample Value	Description	Comments and Units
(0018,0050)	3	Slice Thickness	The nominal slice thickness, in mm. [a]
(0018,0060)	120	kV	The peak tube potential of the x-ray generator, in kilovoltage.
(0018,1150)	500	*t*, Exposure Time	The time of x-ray exposure in msec. [b]
(0018,1151)	187	*I*, X-ray Tube Current	X-ray tube current in mA [c]
(0018,1152)	170	Q, Exposure	The exposure expressed in mAs, which is calculated as the product of the exposure time and x-ray tube current. [d]
(0018,1160)	FLAT	Filter Type	The label for the type of filter inserted into the x-ray beam.
(0018,9306)	0.6	*T*, Single Collimation Width	The width of a single row of acquired data (in mm).
(0018,9307)	12	*NT*, Total Collimation Width	The width of the total collimation (in mm) over the area of active x-ray detection.
(0018,9309)	13.2	*v*, Table Speed	The table speed (in mm/s) during the gathering of data that resulted in this frame. [e]
(0018,9310)	6.6	Δd, Table Feed per Rotation	The motion of the table (in mm) during a complete revolution of the x-ray source around the gantry orbit.
(0018,9311)	0.55	*p*, Spiral Pitch Factor	The ratio of the table feed per rotation (0018,9310) to the total collimation width (0018,9307).
(0018,9323)	Z_EC	Exposure Modulation Type	A label describing the type of exposure modulation used for the purpose of limiting the dose.
(0018,9324)	15.3	Estimated Dose Saving	A percent value of dose saving due to the use of exposure modulation type (0018,9323). A negative percent value of dose savings reflects an increase of exposure. [f]
(0018,9345)	31.9	$CTDI_{vol}$	Computed Tomography Dose Index ($CTDI_{vol}$), in mGy according to IEC 60601-2-44, Ed. 2.1 (clause 29.1.103.4). The Volume $CTDI_{vol}$ describes the average dose **for this frame (image)** for the selected CT conditions of operation.

[a] The reconstructed image thickness is the nomenclature used in this report instead of slice.
[b] How this field is used is vendor-dependent and may not represent the time of one full tube rotation. (0018, 9305) is defined to be the time for one gantry revolution, but is not always utilized.
[c] How this field is used is vendor-dependent. For tube current modulated scans, the value reported here may be the average tube current over a full rotation, but this may vary by vendor.
[d] How this field is used is vendor-dependent. For some vendors, this may be used to represent the product of the exposure time and x-ray tube current; for others it may be used to represent the "effective mAs" or "mAs/slice," which is defined to be the product of rotation time and average x-ray tube current divided by the spiral pitch factor.
[e] Velocity is the nomenclature used in this report instead of speed.
[f] It is not clear what the percentage value of dose saving is relative to. It is most likely vendor-dependent.

In the DICOM image header, $CTDI_{vol}$ is reported for each reconstructed image. An average $CTDI_{vol}$ over an entire CT scan is not reported directly in the DICOM header data of any single image, but can be determined by averaging the $CTDI_{vol}$ from all reconstructed images.

Currently, there is no complete description of tube current modulation (TCM) supplied by CT manufacturers as DICOM data. However, the DICOM image header data do contain, in tag (0018,1151), the tube current value averaged over all projections used in the corresponding reconstructed image. These average tube current values per image, when plotted against the longitudinal patient axis, describe the longitudinal (z-axis) TCM.

AAPM Report 220 strongly recommended that CT manufacturers provide the complete TCM profile, specifically the instantaneous x-ray tube current as a function of projection angle (e.g., every 1 or 5 degrees) and longitudinal position.[27] This will allow modeling of TCM in three dimensions and would be appropriately stored in the DICOM RDSR rather than the DICOM header data of any particular image, as the TCM profile describes the data acquisition as a whole.

2.6 Size-Specific Dose Estimates (SSDE) and Water-Equivalent Diameter (WED)

AAPM Report 204 introduced a method for estimating the absorbed dose at the center of the scan volume to a patient of a specific size. This value, SSDE, makes use of the scanner-reported $CTDI_{vol}$ and conversion factors that take patient size into account.[28] For a given water-equivalent-diameter (WED),[27] SSDE is calculated using a scanner-reported $CTDI_{vol}$ as

$$SSDE = f_{WED} \cdot CTDI_{vol}\,. \tag{8}$$

Here, f_{WED} represents a conversion factor reflecting patient size.[27,28] Although AAPM Report 204 does not specifically use the term WED, the effective diameter values used in Report 204 to determine f_{WED} were for water- or tissue-equivalent materials. AAPM Report 220 clarifies that the effective diameter values used in AAPM Report 204 are, therefore, equivalent to the WED values used in AAPM Report 220.[27] Report 220 further demonstrates that WED can be calculated using either the CT localizer radiograph or axial images reconstructed using a full field of view.[27]

2.6.1 SSDE and Longitudinal Variations in Patient Dimension

Patient dimension and attenuation can vary considerably along the longitudinal axis. When TCM is used, scanner output also varies along the longitudinal (z) axis of a patient, according to changes in patient attenuation. For a cylindrical CTDI phantom, the $CTDI_w$ normalized to a constant tube-current time product ($CTDI_w$ / mAs) is easily measured or can be determined from the scanner's accompanying documents. The instantaneous mAs at every z-axis table position, expressed as *mAs(z)*, is determined by the scanner according to the specific TCM profile used by the scanner. By multiplying the spatially invariant $CTDI_w$ / mAs by *mAs(z)* and dividing by pitch (for a helical scan), the scanner output at each location can be calculated. This information can be recorded as a series of mean $CTDI_{vol}$ values for each reconstructed image, which is referred to as $CTDI_{vol}(z)$. SSDE can be calculated at each position z along the longitudinal direction as

$$SSDE(z) = f_{WED}(z) \cdot CTDI_{vol}(z), \tag{9}$$

where f_{WED} (z) is the size-specific conversion factor from AAPM Report 204 or 220.[27,28] The mean SSDE over the entire scan range can be expressed as

$$\overline{SSDE} = \frac{\sum_{Z=1}^{N} SSDE(z)}{N}, \tag{10}$$

where N is the total number of images. This approach calculates $WED(z)$ and $SSDE(z)$ for each reconstructed image, determining the mean SSDE over the scan range using the $f_{WED}(z)$ and $CTDI_{vol}(z)$ at each longitudinal position.

Leng et al. showed that the mean SSDE over a scan range calculated using Equations (9) and (10) correlated well with a mean SSDE calculated using the WED from a central image in the scan range and the mean $CTDI_{vol}$ over the entire scan range.[29] Thus, for the purpose of estimating a single SSDE value for a given patient, the "shortcut" of using the scanner-reported mean $CTDI_{vol}$ and the WED from a central image in the scan range appears acceptable. AAPM Task Group 246 and EFOMP recommend that $WED(z)$ be provided for each reconstructed image in a standardized DICOM tag, which would provide future opportunities to better estimate organ doses.[30,31]

Using the SSDE, a small patient is correctly attributed a relatively higher absorbed dose compared to that received by a large patient when the same $CTDI_{vol}$ is applied. The SSDE concept takes the scatter tails of the dose profile into account, as the conversion factors f_{WED} were calculated or measured for examinations of typical scan lengths, based on patient size. SSDE has been shown to estimate the mean dose in the center of the scan volume for both constant tube current and modulated tube current acquisitions.[32–34]

2.6.2 Calculation of WED

Calculation of SSDE requires knowledge of the patient WED, either at the center of the scan range, as an average for a certain anatomical region (e.g., thorax, abdomen, or pelvis), as an average over an organ-specific region (e.g., liver), or at the reconstructed image level.

Conceptually, the simplest approach to determining patient size uses the CT localizer radiographs (AP and lateral views) to calculate the WED of the patient. The patient's outer surface is always present in the CT localizer views, while it is not always included in axial image reconstructions, depending on operator selection of anatomy to be reconstructed and the patient size. However, the pixel values in CT localizer image(s) are not provided in absolute units, which means that attenuation and pixel values may not correlate well between different CT manufacturers.[35] Furthermore, CT localizer image(s) are typically presented with significant edge enhancement, which can result in a nonlinear relationship between pixel value and attenuation. Thus, the CT localizer radiograph is difficult for the medical physics community to utilize in the estimation of WED. Manufacturers, however, have the needed tools to estimate WED from the CT localizer radiograph and, in some cases, provide this information in the DICOM image header or the RDSR.[36] Finally, accurate centering of the patient in the gantry is *very* important, since off-center CT localizer radiographs make the patient, as well as the estimated attenuation, appear larger or smaller, respectively, depending on centering in relation to the x-ray tube and detector.

Both ICRU Report 87 and Report of AAPM Task Group 220 provide detailed information on methods to determine the WED from reconstructed image data.[7,27] These methods use CT number thresholds to segment the patient contour and then determine the average pixel density relative to water.[7,27]

3. Current and Emerging Methods to Estimate Organ Dose

There are several different approaches that have been used to estimate organ dose from CT examinations. The most straightforward and easily adoptable is the SSDE, which has been investigated extensively in the literature, as described in section 3.1.

Monte Carlo simulations, which require knowledge of and access to special software, are often used to create the reference standards for organ dose estimation. Using this approach, it is possible to model both the individual patient (either via the actual CT images or mathematical anthropomorphic

phantoms), the actual x-ray beam (kV, collimation, etc.), and conditions of irradiation (axial, helical, etc.). There are also more straightforward solutions, where Monte Carlo organ dose estimates are tabulated for generalized patient types, and the user can select technique parameters and scanner models. These methods are described in section 3.4.

An intermediate solution, between the SSDE and Monte Carlo simulation in complexity, is the convolution method described in section 3.3. Here, dose profiles (e.g., Figure 1) are used together with data on the constant or modulated tube current used for a given CT scan to model the x-ray beam and account for the scatter radiation contribution throughout an entire examination. Since the convolution method employs dose profiles, either measured or simulated in cylindrical phantoms, it may be adopted as an SSDE derivative, together with WED to account for patient size.

3.1 Studies on the Accuracy and Utility of SSDE in Estimating Organ Doses

3.1.1 Typical Head and Body Examinations (Contiguous Axial and Helical)

3.1.1.1 Pediatric

Moore et al. investigated the applicability of SSDE in pediatric CT examinations using physical anthropomorphic phantoms (representing children 5 to 55 kg) and MOSFET dosimeters for direct organ dose measurements in the chest and abdominopelvic regions.[37] The SSDE was determined according to AAPM Report 204 and compared to measured dose for 23 different organs, resulting in organ-specific conversion factors that could be used to determine organ dose given a value of the SSDE.

The authors used the organ-specific conversion factors in a retrospective estimation of organ doses in chest and abdominopelvic pediatric CT examinations, and the results were compared to previously published organ doses on the same examinations from Monte Carlo simulations. The authors found that, for both constant tube current and with TCM, the average agreement between SSDE and absolute organ dose was within ±10% for organs fully covered by the scan volume. However, the organ dose for partially irradiated organs and tissues, e.g., the liver in chest examinations, had a poor correlation with SSDE, resulting in underestimation of organ dose. This is consistent with the recommendations of AAPM Report 204, which states that when the organ is fully contained in the scan volume, SSDE can be used as an estimate of organ dose.[28]

3.1.1.2 Head–Eye Lens and Brain Dose

McMillan et al. and Hardy et al. have extended the SSDE concept for body CT examinations to include head CT examinations.[38,39] Eight patient models (two pediatric patients, three adult males, and three adult females) from the GSF family of voxelized phantoms were used in Monte Carlo simulations of both axial and helical scan modes to achieve conversion coefficients for organ dose (lens of the eye and the brain) from geometric and attenuation-based estimates of head size (effective diameter and WED, respectively) and $CTDI_{vol}$.[40]

The authors report on the strong relationship (axial and helical: $R^2 > 0.92$) between dose to the brain determined by Monte Carlo simulation, as normalized by $CTDI_{vol}$, and all head SSDE values.[38] They concluded that the SSDE concept might be extended to include brain dose estimations.[38,41–43] The relationship was not as strong for dose to the lens of the eye (axial: $R^2 > 0.73$, helical $R^2 > 0.84$). The authors hypothesized that the weaker relationship in results for the lens of the eye might reflect that this small peripheral organ was subject to surface dose variations not included in the simulated model.[38]

It is essential to take into account CT device features that use adaptive shielding and angular, or organ-based, TCM to protect the patient's eyes, or the use of bismuth-containing eye shields.[44–46]

3.1.1.3 Chest–Lung and Breast Dose

SSDE is expected to yield acceptable estimates of absorbed dose for fully irradiated organs in routine thorax examinations provided that patient "size" was determined using WED, as recommended by AAPM Report 220.[27] When only geometric dimensions are considered, errors of up to 20% may occur.[28] This is larger for thoracic examinations than for abdominopelvic examinations due to the presence of lung tissue. Numerous studies have shown that with use of WED, the agreement between SSDE and absorbed dose to fully irradiated organs in the thoracic region is indeed below the 20% tolerance value noted in AAPM Report 204, and often much smaller.[47,48]

As in x-ray mammography, the glandular portion of the breast tissue is the focus of patient-specific breast dosimetry with CT imaging.[49–59] Khatonabadi et al. studied the relationship between average glandular doses normalized by global, regional, or organ-specific $CTDI_{vol}$ values.[60] Correlations between patient size (effective diameter) and normalized breast glandular dose were observed when the scanner-reported $CTDI_{vol}$ was adjusted to take into account TCM along the scan length by using regional or organ-specific average tube current.[60]

Bostani et al. found a good correlation between reference doses determined by Monte Carlo simulation and region-specific normalized average glandular dose when patient size was observed using the effective diameter.[30] The group found that region-specific $CTDI_{vol}$ predicted the breast glandular dose for the cases they investigated to within an average of 9.8%, with minimum and maximum errors ranging from 0.6% to 34%, when compared with Monte Carlo dose calculations.[30]

3.1.1.4 Abdomen and Pelvis

Measurements by Wang et al.[61] and Mueller et al.[62] have demonstrated that SSDE can provide accurate estimates of dose to fully irradiated abdominopelvic organs in constant tube current examinations. In the CT colonography study by Mueller et al., SSDE was compared to dose measured using TLDs placed within the inferior colon *in vivo* during screening CT colonography in a pilot project of 10 patients.[62] The SSDE was found to be on average within 8% of the measured value.[62] This study confirmed the accuracy of SSDE predictions to fully irradiated abdominopelvic organs in general, and to the colon in particular. The absorbed dose to the kidneys, liver, pancreas, and spleen can also be appropriately represented by the SSDE.

3.1.1.5 Fetal Dose

SSDE can be used to approximate fetal dose, as demonstrated by Angel et al., where maternal perimeter at the level of the fetus was used as a metric of patient size.[63] Complexity arises in estimating fetal dose when the fetus is only partially irradiated. In such a case, the SSDE serves as an upper limit of dose to the fetus.

The Monte Carlo-based study using actual CT image data found that patient circumference displayed a strong relation to fetal dose, thus giving further support to the robustness of a SSDE approach.[63] However, they also found that including the fetal depth (distance from skin surface) in a model of fetal dose had a better agreement to the Monte Carlo results than a one-dimensional approach using only a patient size metric.[63] This indicates that the SSDE concept can be further refined to a two-dimensional quantity in order to improve the accuracy of fetal dose estimates.

3.1.1.6 Thyroid Dose

The most radiosensitive organ in neck CT examinations is the thyroid.[4] A method to estimate thyroid organ dose, comparable to a regional SSDE methodology, has been proposed by Huda et al.[64] The method was applied to 11 adult patients, where a neuro radiologist was consulted to specify size and location of the thyroid in each patient.[65]

The average $CTDI_{vol}$ used for the examinations was 26 ±6 mGy, while the TCM increased the tube current by an average of 44% over the thyroid.[65] Estimated thyroid doses ranged from 29 to 80 mGy, with an average of 55 ±19 mGy.[65] These findings suggest that the $CTDI_{vol}$ (and consequently also the SSDE) is a poor metric to estimate thyroid dose. Further refinement is needed to increase the accuracy of (thyroid) organ dose estimates, e.g., by taking TCM into account. Also, for organ dose estimates in the neck region, it is important to note which CTDI formalism is being used, i.e., 16- or 32-cm diameter phantom.

3.1.2 Perfusion Examinations

3.1.2.1 Brain Perfusion

Brain perfusion examinations differ greatly from routine imaging of the brain. With perfusion examinations of the brain, the table is stationary or motion is limited to a small z-axis extent, and exposures are intentionally obtained to image the same anatomy over time. The eyes may or may not be in the primary beam.

Lens Dose

Dosimetry for perfusion also differs from that of a routine brain acquisition. The use of a regional exposure geometry, i.e., 4 or 8 cm, for perfusion imaging, results in the reported $CTDI_{vol}$ that overestimates exposure to the lens of the eye and skin dose due to a lack of scatter x-ray equilibrium that is assumed with the $CTDI_{vol}$ metric. Zhang et al. have shown in simulations for which the eye lens was located fully within the scanning FOV that the $CTDI_{vol}$ overestimates the lens of the eye dose by up to a factor of 1.7.[66]

More recently, an experiment that looked at lens of the eye dose was performed by Lopez-Rendon et al.[67] With the help of a pathologist, 35 thermoluminescent dosimeters (TLDs) were carefully placed at different places (brain white and gray matter, skin, thyroid, salivary glands, oral mucosa, bone surface, and eyes lens) in a female adult cadaver head. The head was subsequently scanned using the clinical protocol for brain perfusion. The measured lens dose was 216 mGy for the right eye receiving direct exposure and 154 mGy for the left eye, which also was directly exposed but was angled differently in the gantry; the average of the two eye lenses was 185 mGy. With a reported $CTDI_{vol}$ of 260 mGy, an overestimation of the eye lens dose was 17% for one eye and 41% for the other eye. On average, the direct exposure to the two eyes was approximately 29% less than the reported $CTDI_{vol}$. The results are similar to those obtained by Zhang et al. and confirm that $CTDI_{vol}$ is a conservative measure of the eye lens dose when used for conventional perfusion-type acquisitions.[68]

Peak Skin Dose

The findings for dose to the lens of the eye from the above studies were similar to those for peak skin dose, i.e., skin dose had approximately the same dependencies on $CTDI_{vol}$ for the scanner type used by Lopez-Rendon et al.[67] Bauhs et al. have shown a point dose method for measuring skin dose with head perfusion examinations.[22] Their results indicated that $CTDI_{vol}$ overestimates skin dose by approximately a factor of 2.

Importantly, these results do not apply to whole-head imaging or to CT-guided biopsy of the brain. Whole-head imaging results in a widely different case of scatter equilibrium than does perfusion imaging. For CT biopsy of the brain, the brain may be positioned lower in the gantry, resulting in a portion of the brain being possibly shielded by the shape of the bow-tie filter. The lens of the eye and a portion of the skin will likely receive a higher exposure level than with the head centered at isocenter.

3.1.2.2 Body Perfusion

CT perfusion examinations of the body are usually associated with higher radiation dose ($CTDI_{vol}$) but are performed with little or no table travel compared to conventional CT imaging. Skin damage or loss of hair from x-ray exposure could occur in extreme cases, such as patients having multiple CT perfusion examinations or interventional fluoroscopy procedures within a few days, or if scan techniques are set incorrectly.[69] The patient table does not translate with most perfusion examinations, and the skin dose distribution differs from that of helical scans.[22]

Recently de las Heras et al. demonstrated a method for converting $CTDI_{vol}$ (measured and device-reported values) into actual peak skin dose using four different CT scanners.[70] The authors concluded that the $CTDI_{vol}$ for the investigated scanners and scan modes can be used to estimate patient-specific skin dose.

Leng et al. measured peak skin doses in shuttle-mode, body perfusion examinations on the anterior and lateral surfaces of tissue-equivalent body-shaped phantoms.[71] Phantoms ranging from 20 to 50 cm wide were used to represent patients from a 10-year-old child to a large adult. For each scan, console $CTDI_{vol}$ was recorded, and the ratio between measured surface dose and console $CTDI_{vol}$ was calculated. Regression analysis was used to determine the dependence of skin dose on patient size. Skin dose was exponentially related to patient size by

$$\text{skin dose} = a \cdot e^{-b \cdot CTDI_{vol}} \; (R^2 > 0.97).$$

The fitting coefficients depended on kV and scanner type, with slight differences between 100 and 120 kV, and large differences for 80 kV. Surface dose expressed as a percentage of $CTDI_{vol}$ at 120 kV varied from 49% to 65% on the 64-slice scanner at 12×0.6 mm collimation and from 86% to 116% on the 128-slice dual-source scanner at 32×1.2 mm collimation across patient sizes. The method used in this study is similar to that of the SSDE approach, i.e., using the $CTDI_{vol}$ and metrics of patient size to determine organ (skin) dose. While SSDE estimates the average dose at the middle of the scan range, this study estimated skin dose from perfusion scans.

3.2 Organ Dose Estimates with Regional $CTDI_{vol}$ Values

For the task of estimating organ doses, Khatonabadi et al. compared the accuracy of regional SSDE (i.e., the SSDE calculated using the $CTDI_{vol}$ averaged over a specific anatomic region) to that of the scan-averaged SSDE (i.e., the SSDE calculated using the $CTDI_{vol}$ averaged over the entire scan volume).[31] The authors used Monte Carlo simulations and actual helical CT image data, acquired using TCM, to determine the reference absorbed dose in five different organs (liver, spleen, kidneys, lungs, and glandular breast tissue for female patients) to benchmark the accuracy of the different SSDE approaches for estimating organ dose.[31] They found that the SSDE calculated using the scan-averaged $CTDI_{vol}$ was in poor agreement with the Monte Carlo results. When the SSDE was determined using the $CTDI_{vol}$ and an image-by-image approach, Equations (9) and (10), either for a region (e.g., abdomen) or a specific organ (e.g., liver), the correlation to the Monte Carlo results was stronger.[31] The best agreement between Monte Carlo results and SSDE organ dose estimates based on SSDE occurred with the organ-specific approach, which is a logical finding. However, even the estimates based on regional SSDE were found to be an improvement compared to the estimates made using the $CTDI_{vol}$ averaged over the entire scan.

3.3 Application of the Convolution Method for Organ Dose Estimation

As described in section 2, $CTDI_{100}$ does not adequately account for the entire dose delivered by scattered radiation. Any derivative of $CTDI_{100}$ inherits this limitation. Thus, $CTDI_{vol}$ underestimates the equilibrium dose by an amount that depends on patient size, examination scan length, and x-ray beam collimation width.

Dixon has presented a convolution method for dose estimation that takes into account the complete scanner profile.[72] In the simplest form (constant tube current), the method uses dose profiles *f(z)*, either calculated or measured with a small-volume ionization chamber, to characterize the x-ray beam and scatter tails in a cylindrical dosimetry phantom. The accumulated dose distribution, *D(z)*, from a CT scan can then be determined by convolution:[72]

$$D(z) = \frac{1}{\Delta d}\int_{-L/2}^{L/2} f(z - z')dz' = \frac{1}{\Delta d} f(z) \otimes \prod(z / L). \tag{11}$$

Here, L represents the total CT scan length and Δd the table advance per rotation. Note that by setting $z = 0$ (center of scan length), $L = 100$ mm, and $\Delta d = NT$ (a pitch of unity), Equation (11) reduces to $CTDI_{100}$. The formalism described by Equation (11) can be demonstrated graphically, as shown in Figure 2.

The method described in Equation (11) takes the axial dose profile *f(z)* for a single rotation (blue line) and convolves it with a box function $\Pi(z / L)$ to yield the accumulated dose distribution *D(z)* in a cylindrical dosimetry phantom (red dashed line). The box function tells us how the dose profile is added to the accumulated dose distribution at each point z. Thus, Equation (11) gives a description of a constant tube current CT scan of length L in a homogeneous cylinder of water. The user input to describe the accumulated dose distribution requires three parameters: the dose profile for a single revolution of the x-ray tube resulting from specific scan parameter settings (e.g., a specific nominal beam collimation and x-ray tube potential), the table advance per rotation, and the total scan length. Thus, two pieces of the information needed to complete the calculation described in Equation (11) can be found in the DICOM metadata. The obvious limitation with application of the convolution method is that dose profile information is not readily available to the medical physics community. Dixon and Boone, however, have derived analytical equations for the dose profile *f(z)* for the 32-cm PMMA (body) phantom.[73] The convolution method is not limited to describing constant tube current scans. To model a helical scan acquired using TCM, Equation (11) can be modified to use the x-ray tube current

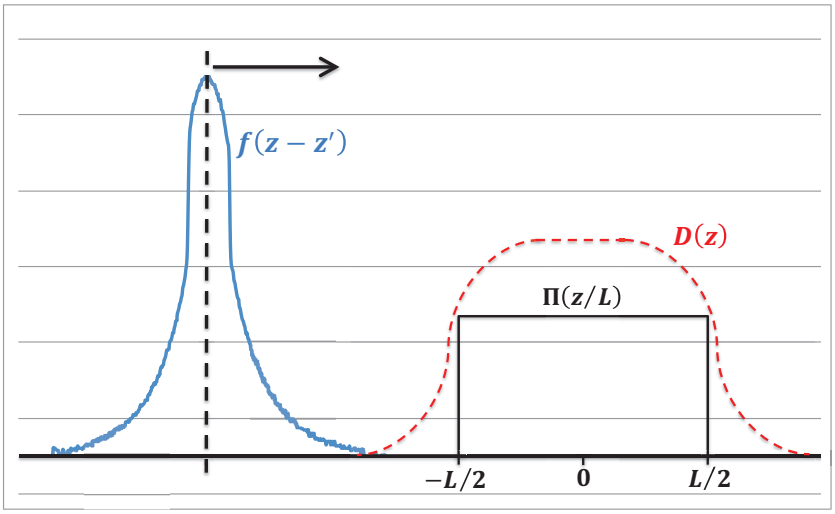

Figure 2. A graphical representation of the convolution method, adapted from Dixon.[72] Here a dose profile *f(z)* is convolved with a box function to represent a constant tube current scan.

at each z-axis location, *i(z'),* such that the dose profile contribution for each tube current strength *i(z)* is added,

$$D(z) = \frac{1}{\Delta d}\int_{-L/2}^{L/2} i(z')f(z-z')dz' = \frac{1}{\Delta d} f(z) \otimes \left[i(z)\prod(z/L)\right], \quad (12)$$

where $f(z)$ is the dose profile per unit value of the tube current. The physical interpretation of Equation (12) is that the dose at z depends on the tube current $i(z')$ at all locations over the entire scan length L. The addition of a description on how the x-ray tube current varies in the z-axis over a CT scan in the convolution, Equation (12), thus makes it possible to determine the accumulated dose distribution for spiral CT scans with TCM. Dixon et al. has described the difference between estimating dose according to the convolution method for constant tube current and TCM, which is shown in Figures 3 and 4, respectively.[74]

Figures 3 and 4 describe a constant tube current scan and TCM CT scan, respectively; the scan lengths were identical, and the average tube current for the TCM scan was equal to the constant tube current scan. Since the IEC method for computing $CTDI_{vol}$ treats the average tube current over the entire scan length as if it were a constant tube current, then both have identical values of scanner-reported $CTDI_{vol}$. The SSDE will differ between the two examples, however, because both *i(z)* and *f(z)* are determined by the value of *WED(z)* in the case of TCM, whereas only *f(z)* varies with *WED(z)* for a constant tube current scan.

Recently, Tian et al. evaluated the convolution method for use with TCM in 60 clinical patient examinations.[75] The results were benchmarked against Monte Carlo simulations to estimate patient organ dose accuracy. For the Monte Carlo simulations, each patient was matched to a representative

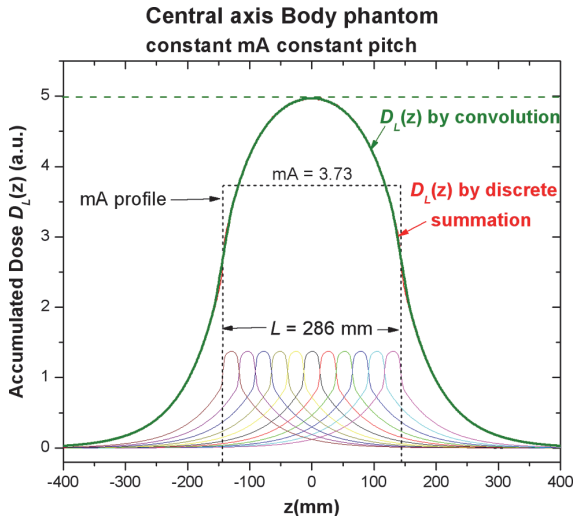

Figure 3. An example of the convolution method used for a constant tube current (mA) scan. Characterization of the accumulated dose profile was done for the central axis of a body dosimetry phantom.[74] The accumulated dose profile was calculated by convolution of the dose profile for a single rotation (the small colored profiles) with a box function per Equation (11).

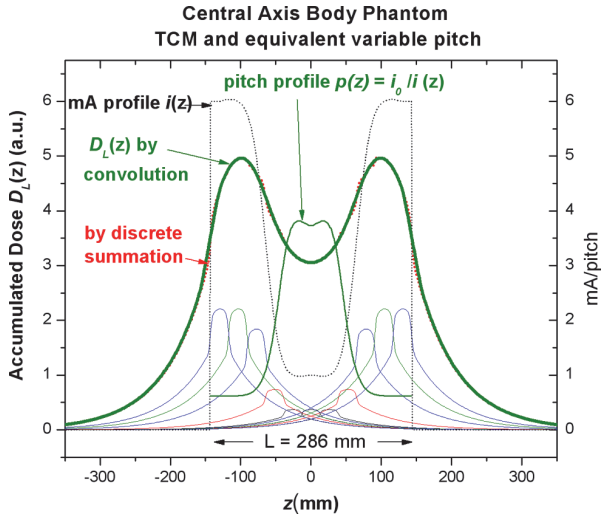

Figure 4. An example of the convolution method used for a TCM CT scan. Characterization of the accumulated dose profile was done for the central axis of a body dosimetry phantom.[74] In this extreme example, the dose profile for a single rotation, *f(z),* (including its long scatter tails) is scalable by the regional tube current (mA), whereas the accumulated dose distribution is not due to scatter tail contributions from other dose profiles over the scan length.

computational phantom.[76] To model the impact of TCM in the Monte Carlo simulations, the tube current profiles were estimated for each computational phantom.[77] The convolution method was used together with a Monte Carlo-modeled dose profile representative of the maximum x-ray beam collimation of the scanner on the central axis in an infinitely long 32-cm-diameter CTDI phantom. The dose profile was convolved with TCM profiles to generate accumulated dose distributions for 60 clinical patients. Simulations of constant tube current were also performed for each patient to normalize regional and organ dose to $CTDI_{vol}$ and compare results from the convolution method and Monte Carlo simulations, respectively. The patient size was known for each subject through the computational phantom matching for Monte Carlo simulation employed by Tian et al.[75] Exponential regression models were used to determine organ dose as a function of patient body diameter. Since the distribution of organs was already estimated from matching to computational phantoms, organ dose estimation by the convolution method was straightforward in this work. Tian et al. found that organ doses estimated by the convolution method were generally within 10% of the Monte Carlo simulation results.[75] Larger deviations for the convolution method were found for the shoulder and pelvic regions. Tian et al. also found that compared to a full Monte Carlo simulation, the estimation method using a global $CTDI_{vol}$ based on the average tube current of the entire examination yielded a poor estimate of organ dose, with a maximum error above 50%, similar to the results reported by Khatonabadi et al.[31,75] By comparison, the method based on the approximation that regional dose depends on regional tube current significantly improved the accuracy of organ dose estimation, again similar to the results reported by Khatonabadi et al.[31] The convolution method provided the most accurate estimation across patient models and TCM strengths, since it most accurately accounted for scatter emanating from the entirety of the scan length.[75]

The convolution method cannot use the SSDE formalism discussed in AAPM Report 204[28] since dose profiles are used to describe the primary x-ray beam and scatter radiation instead of the $CTDI_{vol}$. However, similar correction factors for patient size, related to standard phantoms used for measuring or simulating dose profiles, can be derived for the convolution method.

3.4 Monte Carlo Simulation Methods

There has been a substantial history of the use of Monte Carlo-based methods to estimate patient dose from CT examinations.[16,17] These methods require several components. The Monte Carlo simulation code models the stochastic properties of x-ray interactions with tissues (e.g., photoelectric and Compton scatter interactions), which is adapted to estimating organ doses. Monte Carlo simulation requires:

(a) modeling the x-ray source's spectra, filtration, and geometry;

(b) a model of the patient's anatomy, and specifically the organs of interest;

(c) a description of the scan parameters, including start and stop locations, as well as elements such as helical path; and

(d) a mechanism to transport photons through the geometry and tally doses to the organs of interest.

These are described below.

3.4.1 Monte Carlo Engines and Computational Phantoms

A growing number of CT scanners are being modeled for use with Monte Carlo radiation transport codes, where device-specific refinements in modeling exposure conditions improve estimates of patient radiation dose through advanced modeling of the x-ray beam and irradiation geometry.[78–86]

A computational anatomic phantom is a computerized representation of human anatomy in a format amenable to coupling with Monte Carlo radiation transport codes. These codes are computer programs that use random sampling of probability distributions of radiation interaction type (scatter or

absorption), energy transfer (full or partial), and scatter/emission angles to follow individual x-ray photons, and potentially their secondary electrons, from a simulated model of the CT x-ray source through the simulated model of patient—the computational phantom.

During Monte Carlo radiation transport of x-ray photons within a computational phantom, energy deposition is scored within spatial regions associated with individual organs. Organ absorbed dose is thus reported as the ratio of the scored energy deposition and the phantom organ mass. The one general exception is for estimates of absorbed dose to the active (or red) bone marrow and the bone endosteum. For these skeletal tissues, the microscopic structure of the bone trabeculae and individual marrow cavities is generally too small to be properly represented in a computational phantom. One solution is thus to score, not energy deposition, but energy-dependent photon fluence in these skeletal regions, and then convolve those fluences with an energy-dependent and bone-specific fluence-to-dose response function. Photon dose-response functions are presently available for adult phantoms in a work by Johnson et al. and Annex D of ICRP Publication 116.[87,88]

Individual computational phantoms have two defining characteristics—their format type and their morphometric category. Format types include stylized, voxel, or hybrid forms. Stylized (or mathematical) phantoms are composed of 3D geometric surface equations defining both internal organ anatomy and the external body profile. Individual organs are composed of various geometric objects such as spheres, ellipsoids, and cones, either as single entities or as geometric combinations. Voxel phantoms are composed of a 3D array of voxels of labeled anatomy that are typically based upon the segmentation of medical images (CT, MR, etc.) of patients or cadavers. Hybrid models preserve the anatomical realism of a voxel phantom and are typically modeled through either NURBS (nonuniform rational B-spline) or polygon mesh surfaces.

Morphometric categories include: reference, patient-dependent, patient-sculpted, and patient-specific. A reference phantom is one in which the morphometry is defined formally, such as the reference male and female phantoms established by the International Commission on Radiological Protection,[89,90] which describe the 50th percentile individual in both height and weight at a given age and gender. Patient-dependent phantoms are similar to reference phantoms, but with the removal of the restriction of 50th percentile height/weight. This allows the creation of a phantom library, whereby a specific member from that library may represent, for example, a female patient at 30th height percentile and 65th weight percentile at a specified age. Patient-sculpted phantoms typically start from patient-dependent phantoms and then reshape the outer body contour (typically using NURBs or meshes) to more closely match the body shape of the individual patient for which CT organ doses are to be assessed. Finally, patient-specific phantoms are those in which both internal organ anatomy and outer body shape is uniquely matched to the patient for which the organ dose estimate is sought (such as in voxel phantoms).

Once a particular patient phantom model is selected for CT organ dose assessment for a specific patient, several steps are needed to complete the computational model of the imaging system. These steps are briefly outlined below.

3.4.2 Modeling of the X-ray Source

In a Monte Carlo simulation of a CT imaging examination, one must specify the starting position, emission direction, and energy of each simulated x-ray photon within the virtual imaging beam. Depending upon whether axial or helical scanning is considered, Monte Carlo sampling occurs along a simple circle at each exposed position on the phantom, or along a helical path of a selected pitch. Emission direction is sampled within an angle defining the fan beam width, and the beam collimation defines the emission direction with additional consideration of the beam penumbra (i.e., overbeaming).

Early attempts at Monte Carlo modeling of CT imaging required explicit knowledge of the material and geometric shape of the bow-tie filters to properly model the probability density function of emitted x-ray energies. In 2009, Turner et al. published an experimental approach which circumvented the need for this proprietary information.[91]

3.4.3 Monte Carlo and Normalization of Reported Organ Dose

Measurements are generally required for estimating organ doses to patients from Monte Carlo simulation. The direct output of Monte Carlo simulations typically yields organ doses per simulated x-ray photon (mGy/photon), while the organ dose is reported as dose per time-integrated tube current (mGy/100 mAs). Thus, a normalization factor is required to provide the number of x-ray photons per 100 mAs for a given irradiation geometry, typically one single axial rotation. This normalization factor can be calculated as the ratio of measured and simulated $CTDI_w$, respectively.[92,93]

3.4.4 Generic Axial Dose Libraries vs. Helical Protocol-Specific Dose Libraries

Under the basic approach of organ dose determination employing computational phantoms and Monte Carlo simulation, two options exist for establishing a precomputed CT organ dose library. The first option establishes an organ dose library based upon Monte Carlo simulation of an array of single-rotation axial images at a given collimation beam width, tube potential, and a given selected computational phantom. This axial acquisition dose library provides the organ dose, typically normalized to 100 mAs, indexed to each z-position in the computational phantoms, and can in theory extend across the entire craniocaudal length of the virtual patient. For a given clinical imaging examination, one then linearly sums the z-level specific organ doses over all axial acquisitions that fall within the starting and ending anatomy of the CT examination.

For modeling helical protocols, the summed organ doses are scaled by the inverse of the examination pitch. This approach thus permits explicit consideration of any combination of starting and ending anatomical landmarks. In the second option, when CT imaging studies fall under a specific listing of established clinical protocols, and where the anatomical landmarks of the scan length and the pitch of the examination are well established, the CT organ dose library may be constructed for each explicit imaging protocol through explicit modeling of the helical scan.

3.4.5 Considerations of Starting Angle and Overranging

A disadvantage of a protocol-specific organ dose library is that a fixed starting angle is typically assumed during the Monte Carlo simulations of the helical path of the x-ray tube. Variations in CT starting angle may influence doses to more superficial organs, such as breast, thyroid, and eye lens.[94,95] One solution is to consider a systematic variation in starting angle for the helical path protocol-specific dose library, and populate the organ dose library with the organ dose averaged over all possible starting angles. For example, axial acquisition dose libraries consider all possible starting angles and provide the average value. In either case, this dose value may differ greatly from the actual organ dose to superficial organs for a given helical scan with an arbitrary starting angle. Overranging—which defines additional irradiated anatomy prior to and beyond the edges of the reconstructed images—may be accounted for in the organ dose library by incorporating additional (whole or fractional) simulated rotations in the final dose estimate.

3.4.6 Monte Carlo and Modeling of TCM

The incorporation of TCM information into Monte Carlo simulation methods has been described and investigated, both for angular and longitudinal forms by Angel et al.[96,97] The works by Angel et al. used TCM functions from actual scans and, therefore, were only available retrospectively and were specific to the patients being modeled. In addition, Khatonabadi et al. demonstrated that for a combined angular and longitudinal modulation TCM scheme, modeling only the longitudinal modulation

(e.g., using values from the DICOM image header data) provided reasonable estimates for organ doses.[43]

However, one significant challenge to reporting organ doses following CT imaging on a *pre-computed basis* is the impact of TCM—in both its angular and longitudinal forms. While all TCM algorithms are based on the measurement of patient attenuation and the adaptation of tube current to that attenuation, the implementation of various manufacturers' methods are quite different. Manufacturers may use different control parameters (e.g., Quality Reference mAs or Noise Index), relationships between the attenuation and tube current, as well as the ability to have users set minimum and maximum tube current limits, and these may all influence the actual TCM function. One approach to simulate and validate the TCM function from one manufacturer is described in McMillan et al.[33]

3.5 Monte Carlo Simulation with Stylized Anthropomorphic Phantoms

Organ dose estimates using stylized computational phantoms are available from different sources, e.g., the ImPACT CT Patient Dosimetry Calculator, which uses tabulated Monte Carlo data sets from the National Radiological Protection Bureau.[16,17] Patient-specific attributes may be used to match a stylized phantom to a patient. Stylized computational phantoms incorporate the Monte Carlo radiation transport simulation of a representative CT examination. The Monte Carlo simulation depends on basic output (kV, mA, rotation time, pitch, etc.) and also machine-specific factors.

An example for an examination of a standard adult modeled by the NRPB18+ stylized computational phantom for a given CT scanner using ImPACT is given in Figure 5.[98] An average $CTDI_{vol}$ value of 13.3 mGy was found for 2,434 patients receiving a routine abdomen examination (personal

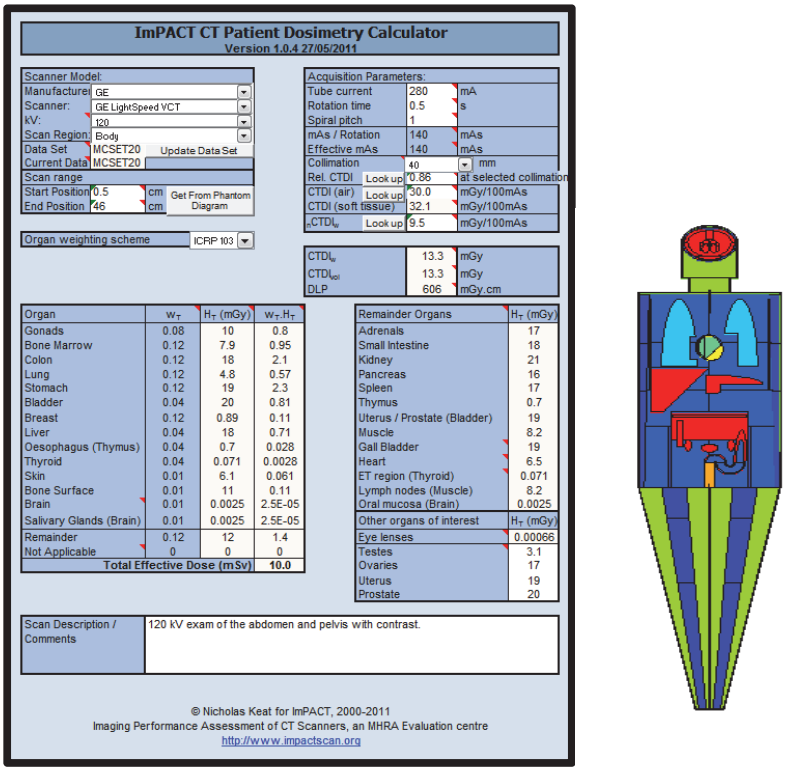

Figure 5 Left: organ dose calculation example from ImPACT CT Patient Dosimetry Calculator. Right: the NRPB18+ stylized computational phantom.[98]

communication, William Pavlicek, Mayo Clinic, Scottsdale, AZ). The average size of patients among the 2,434 examinations measured from the CT localizer radiographs was 28.6 cm in the A-P and 36.3 cm in the lateral direction. These measurements correspond to an effective patient diameter (geometrical mean) of 32.2 cm.

Figure 5 shows the acquisition parameters used to achieve a $CTDI_{vol}$ of 13.3 mGy. The ImPACT CT Patient Dosimetry Calculator gives estimates of absorbed dose for each organ and tissue (H_T), as well as an estimate of total effective dose, which have weighing factors (w_T) defined in the ICRP 2007 recommendations.[4]

The organ dose estimates in Figure 5 may be compared to the SSDE; calculating the SSDE for the average-sized patient (effective diameter 32.2 cm) in the example yields a value of 15.2 mGy.[28] As previously discussed, Mueller et al. found that the SSDE was a good estimate of dose to the colon in a comparison with TLD measurements *in vivo*.[62] The present colon dose estimate from the ImPACT Patient Dosimetry Calculator is 18 mGy. The difference between these colon dose estimates is 16%, which may arise in part from approximations in estimating patient size for SSDE. Using WED and $CTDI_{vol}$ for each reconstructed image instead of patient size at a single point in the z-axis and the average $CTDI_{vol}$ for the examination may have improved the estimation accuracy. This underlines the importance of uncertainty estimates in any methodology used to determine organ dose. Uncertainties in organ dose estimates are discussed in section 4.

3.6 Monte Carlo Simulation to Model the Dose Deposited by a CT Scanner

It may be assumed that accuracy can be improved for patient-specific computational phantoms by matching the actual high-resolution imaging data, at least for organs and tissues completely inside the actual imaged volume. However, the segmentation of all organs and tissues necessary for organ dose determination is very challenging, regardless if a manual or automatic approach is considered. Furthermore, scatter, overbeaming, and overranging outside the imaged and modeled volumes (partially or completely) may contribute substantial dose to these organs. Computational phantom models do not have the problem of estimating organ doses outside the imaged volume, but they are limited in their ability to mimic an individual patient. Finally, some small organs are varied in their position in the body (e.g., the location of the ovaries varies within the pelvis). Hence, computational phantoms may not accurately represent the location of such small organs for a given patient.

Recently, Kalender et al. used physical anthropomorphic phantoms—an adult Rando-Alderson phantom (RANDO Phantoms Laboratory, New York, USA), 1-year-old, and 5-year-old child CIRS phantoms (Computerized Imaging Reference Systems, VA, USA)—to explore the effects of scatter and overranging on organ dose.[99] The physical phantoms were imaged emulating thorax scans, and organ doses to various sites were measured with the use of TLDs. Whole-body voxel models of the physical phantoms were built from the CT images appended by data from computational phantom models (ICRP and ORNL phantoms, respectively).

Figure 6 shows the dose distributions from a thorax scan achieved by Monte Carlo simulation of the CT images and the whole-body volumes, respectively, for the adult Rando-Alderson phantom.[99]

The effect of scatter and overranging in the simulated spiral mode thorax scan is obvious in the graphical representation of dose distribution in Figure 6. Organs outside the imaged volume, e.g., the liver and thyroid are examples of organs with a too low of absorbed dose if calculations use only the CT imaged volume. Furthermore, organs and tissues inside the imaged volume are also attributed less absorbed dose due to neglect of scatter from the volume(s) on either side of the scan, as seen when comparing Figure 2.5 (c) and (d), i.e., the CT image volume model assumes that the body ends where the image data starts and stops, respectively.

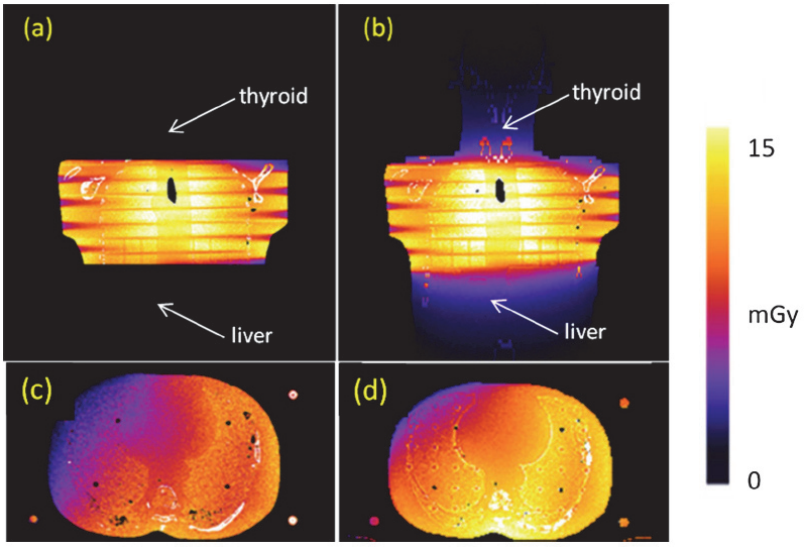

Figure 6. Monte Carlo-simulated dose distributions from a thorax scan for CT image (a, c) and whole-body (b, d) volume, by Kalender et al.[99]

Kalender et al. compared the Monte Carlo results to TLD measurements and found that the CT image model underestimated organ dose by 8% to 15% on average (up to 37%), while results from the whole-body model were within 10% of the TLD measurements.[99]

While the work by Kalender et al. was performed on physical phantoms instead of patients, and quite basic computational models were used to create the whole-body models, it shows the possibilities for future dosimetry approaches.[99] This refined modeling concept and strategy may be used for automatic organ volume segmentation in advanced patient-specific models, incorporation of sophisticated CT scanner models in Monte Carlo simulations, automatic reporting of input data into Monte Carlo radiation transport code, and refined modeling with DICOM metadata for automatic input of patient and CT scanner related parameters.

3.7 Benchmarking and Validation of Monte Carlo Simulations

Monte Carlo simulations are inherently based on models of CT scanners, patients, and examinations. While the modeling can be quite detailed in many instances, a necessary step prior to reporting organ doses should be the benchmarking and validation of the Monte Carlo simulation results under known (e.g., phantom) conditions. There have been several approaches to this, including the creation and use of reference datasets described in AAPM Report 195.[100] In addition, there have been several efforts describing the validation of Monte Carlo simulation results by comparing them to physical measurements in phantoms and even *in vivo* measurements (e.g., TLDs used during CT colonography).[41,42] AAPM Task Group 246 and EFOMP recommend that the steps used to benchmark and validate Monte Carlo simulation results be reported together with organ dose estimates, according to publications by AAPM Task Groups 195 and 268.[100,101]

4. Sources of Uncertainty in Estimating Organ Dose

Among various dose metrics, organ dose is generally regarded as one of the best metrics to quantify individual radiation burden. Since all methods of calculating organ dose estimates are inherently associated with some amount of uncertainty, the factors contributing to the uncertainties associated with

different organ dose estimation methods need to be elucidated and understood. Variations of organ dose estimates for the methods discussed in this report may range up to 50% from a single source. While this uncertainty is small compared to that associated with the estimation of individual risk from specified irradiations (± a factor of 3),[102,103] a quantitative estimate of uncertainty provides a better understanding of the limitations of current organ dose estimation methods and indicates areas for which further research is needed.

AAPM Task Group 246 and EFOMP recommend the inclusion of percent uncertainty data for estimates of organ dose, as well as any underlying assumptions included in the methodology that may yield additional uncertainty. This uncertainty in dose should be determined in as rigorous a manner as possible.[104]

4.1 Uncertainties in SSDE–based Calculations of Patient Organ Dose

Table 3 contains examples of sources of uncertainties in SSDE estimates of patient organ dose discussed in this report. Estimated uncertainties given as percentages are to be understood as indications of the present knowledge. More work is needed to better understand the uncertainties associated with organ dose estimates for CT examinations.

4.1.1 Pencil Ionization Chamber Measurements and $CTDI_{vol}$

The pencil ionization chamber is an accepted and accurate dosimeter when calibrated, and as used in the IEC methodology for quantifying the $CTDI_{vol}$. The physicist can provide improved accuracy when reporting patient organ dose that is based on an independent measure of $CTDI_{vol}$, and consequently also the SSDE, as compared to using the manufacturer's reported values of $CTDI_{vol}$ (DICOM RDSR or Dose Data Page) and their associated tolerances (Table 1).

4.1.2 The SSDE

The SSDE is an appropriate estimate of dose to internal organs fully located within the scanned region. In general, for a constant tube current examination, a physicist can calculate an organ dose estimate for fully irradiated organs for a patient who is centered in the gantry using the SSDE and achieve an uncertainty within ±20%.

Table 3: Summary of selected sources and level of uncertainties that can be expected in SSDE estimates of patient organ dose

Source of Uncertainty	Contributing Factors	Estimated Uncertainty (±)
$CTDI_{vol}$ measured by the physicist using a calibrated ionization chamber	Small differences in phantom dimensions, differences in the energy dependence and calibration reference for dosimeters, reproducibility of measurements by individuals	Up to 5% for measurements made by the same individual, likely 10% to 20% across a range of measurements. The 15% to 40% tolerances used by the manufacturers likely overestimates the uncertainty (see Table 1).
SSDE using geometric measures of patient size	In the thorax, patient size is not an ideal surrogate of patient attenuation due to the presence of large air cavities	Up to 20%
SSDE using attenuation-based measures of patient size	This accounts for uncertainty in $CTDI_{vol}$ and patient size	Up to 10%
SSDE and TCM using the concept of regional $CTDI_{vol}$	This accounts for uncertainty in $CTDI_{vol}$ and patient size	Up to 20%
Assuming that the patient is at isocenter	Bow-tie filter modulates the x-ray beam(s) that exposes the patient; if the CT localizer radiograph is used to estimate patient size for SSDE calculations, the size may be over- or underestimated	Up to 50%, depending on the actual patient centering achieved[105]

4.1.3 SSDE and TCM Examinations

The uncertainty introduced into organ dose estimates from the SSDE by TCM along the z-axis can be reduced by using regional values of the $CTDI_{vol}$ that best describe the irradiation over the organ of interest. However, the SSDE will not properly account for organ dose variation at the patient periphery due to non-uniform irradiation from TCM in the (rotational) xy-plane.

4.1.4 Patient Not Centered in the Gantry

The $CTDI_{vol}$, and consequently the SSDE, may be a poor predictor of organ dose when a patient is positioned either too high or low in the gantry, due to the impact of the bow-tie filter modulation on the x-ray beam, and over- or under-estimation of patient size using a CT localizer radiograph. For routine examinations, the SSDE may under- or overestimate organ dose by as much as 50% when a patient is not centered in the gantry.[105]

4.1.5 The SSDE and Partial Organ Irradiation

The SSDE does not yield accurate estimates of dose for partially irradiated organs. Monte Carlo estimates of organ dose, which are currently considered the gold standard, should be used when tasked with determining dose to partially irradiated organs.

4.2 Uncertainties in Monte Carlo Estimates of Organ Dose

Over the past decade, significant progress has been made in quantifying organ dose with various techniques that make use of Monte Carlo methods.[106–111] The estimation accuracy with such methodology is critically dependent on how well the model represents the individual patient under consideration and the actual examination exposure conditions. Table 4 offers a summary of the sources of uncertainty in Monte Carlo estimates of organ dose. Estimated uncertainties given as percentages are to be understood as indications of the present knowledge.

4.2.1 Computational Phantoms

The uncertainties associated with using computational phantoms have been previously reported in several studies. Zhang et al. assessed the organ dose uncertainties associated with four different computational phantoms (ICRP, CT-Expo, XCAT, and ImPACT) for 10 body and three neurological CT

Table 4: Summary of the sources and level of uncertainties with computational phantoms and Monte Carlo organ dose estimations

Source of Uncertainty	Contributing Factors	Estimated Uncertainty (±)
Computational phantoms	Depends on how accurately different types of computational phantoms resemble the anatomical structure of the actual patient	3–66%
Patient matching	Induced by geometry differences between a patient and the computational phantom that is used to represent that patient	10–15%
Organ start/end location	Induced by the heterogeneous dose pattern created across the body by the helical trajectory of the CT source	<10% for most organs 10–33% for the small surface organs
TCM simplification	Induced by using simplified tube current profiles (z-dimensional) to approximate organ dose under TCM	20% depending on the method used to model the dose field under TCM
Monte Carlo simulation	Mainly caused by the underlying differences in the physical models used by different codes	5–10%
Assuming that the patient is at isocenter	Bow-tie filter spatially changes the assumed x-ray beam if the patient is not centered	Up to 50% depending upon the actual patient centering[105]
Organs partially irradiated	E.g., thyroid, bone marrow, and skin	Depends on the extent of partial organ irradiation

protocols.[112] With one single dose estimation technique used across all phantoms, the average percentage differences were in the range of 3% to 38% for fully irradiated organs and 7% to 66% for partially irradiated organs. Sizable differences were found for organs located near the scan boundary, e.g., testes for abdominopelvic examination and colon for chest examination. Furthermore, noticeable uncertainties were found for organs with different spatial distribution across phantoms, e.g., breasts for female phantoms. Liu et al. compared the organ dose differences between RPI and ICRP reference phantoms for chest, abdominopelvic, and chest-abdomen-pelvis protocols and found that the ratio between the organ doses for the two types of phantoms were within the range of 0.75 to 1.16 for the majority of fully irradiated organs.[113] However, significant differences were found for organs near the scan start/end locations. In both studies, uncertainties were mainly introduced by variation in organ location and spatial distribution.

Tian et al. assessed the uncertainties associated with patient matching to computational phantoms for chest and abdominopelvic examinations.[75] The organ dose differences between the matched patient pairs were on average 11% and 15% for chest and abdominopelvic examinations, respectively. The largest uncertainties were found for small organs near the scan start/end regions, e.g., testes for abdominopelvic examinations and thyroid for chest examinations.

4.2.2 Scanner Irradiation Conditions

The uncertainty associated with scanner irradiation conditions refers to modeling of the scanner irradiation mode, including geometry and physical properties of the CT scanner, scanning collimation, start and end tube angle positions, overranging, table and head holder attenuation, and the TCM technique.

Mostly associated with spiral CT, the uncertainties associated with tube start/end locations are mainly induced by the helical trajectory and the incorporation of 'pitch' (table movement) relative to the CT source. This geometry creates a periodical dose pattern across the patient periphery (see Figure 6). Zhang et al. and Li et al. have studied the effect of tube start/end location under different conditions (e.g., pitch, collimation) for different patient models (infant, small child, adult female, and pregnant patient) and found that the largest dose variations occur for eye lens, thyroid, breasts, and testes, all of which are at or near the surface of the patient.[95] The uncertainties were in the range of 10% to 33% across different phantoms for the small surface organs.

Another main source of organ dose uncertainty is the modeling of TCM, which requires effective quantification of dose field distribution created by the changing tube current. Khatonabadi et al. and Li et al. demonstrated the use of a regional $CTDI_{vol}$ estimated by averaging the tube current values within the organ region to approximate organ dose under TCM.[31,77] The uncertainties associated with such techniques were found to be generally within 20% for most organs, but not organs located in the pelvic and shoulder regions.

In addition to the uncertainty associated with geometry and irradiation conditions of the scan, uncertainty is associated with the statistical fluctuations with any Monte Carlo simulation and the underlying differences in the physical models used by different implementations. The latter uncertainties are generally small and within 5% to 10%. As the organ dose is an average over a large volume of tissue, the uncertainties generally exceed those associated with the statistical uncertainties, which are normally in the range of 1% to 2%.[100]

4.2.3 Patient Not Centered in the Gantry

Monte Carlo methods typically use a computational phantom centered in the simulated CT scanner gantry, while the individual patient may or may not be centered in the gantry. Organ dose estimates from Monte Carlo methods are thus associated with the same additional uncertainties as the SSDE when the patient is not positioned at isocenter. If the bow-tie filter modulation of the x-ray beam is

used in the Monte Carlo model of a CT scanner, and the patient location in the gantry during an examination is reported, it appears possible to correct for this variability.[114]

4.3 Contrast Media Used in CT Examinations

Recently, Sahbaee et al. assessed the dose increase due to the presence of contrast media in CT examinations and found substantial increase of estimated local radiation dose.[115] Furthermore, Tran et al. found an even larger increase of estimated local radiation dose for a standard clinical contrast-enhanced body CT examination compared with a non-contrast examination.[116] To what extent those increased radiation dose values corresponded to increased radiation burden to biological tissue, as opposed to radiation energy being absorbed only to the contrast medium alone, requires further investigation.

4.4 Reporting Uncertainty with Estimates of Patient Organ Dose

AAPM Task Group 246 and EFOMP recognize the importance of including an estimate of the uncertainty in the computation with any report of patient organ dose estimates. It is possible for a reported patient organ dose estimate to indicate which methods, considerations, and underlying assumptions were used in the computation. While the spectrum of patient physical representations, CT scanners, and examination-specific conditions create complex variations in patient exposures, the physicist should report the calculation methods for patient organ dose estimates and indicate the efforts undertaken to improve their accuracy. AAPM Task Group 246 and EFOMP recommend that patient organ dose estimates should be reported with a measure of the associated uncertainty.

5. Summary of Report and Recommendations

The goal of this Joint Report of AAPM Task Group 246 and EFOMP was to assist the clinical medical physicist in estimating individual patient organ doses from CT examinations. We are greatly aided in this endeavor by the continuing efforts of the scientific medical physics community, as well as the emergence and greater availability of the DICOM Radiation Dose Structured Report (RDSR). Furthermore, refined and new dosimetry systems continue to evolve and form the basis for demonstrating accuracy. Information systems capable of handling big data are emerging for large-scale patient dose monitoring and quality assurance tools.

The $CTDI_{vol}$ provides the fundamental radiation dose metric for CT, but it has limitations for estimating patient organ dose because of the lack of specificity regarding patient size that is included in the $CTDI_{vol}$ concept.[28] The normalized dose coefficients detailed in the AAPM Task Group 204 report for computing the SSDE from examination averages of $CTDI_{vol}$ and patient size contain information that increases the robustness of the SSDE for estimating patient organ dose for a given sized patient. AAPM Task Group 246 and EFOMP endorse the recommendations made in AAPM Report 220 on how the WED should be estimated.[27]

The dose to a patient from CT localizer radiographs, while small compared to routine CT examination doses, may be of interest for specific protocols (e.g., pediatric imaging or very-low-dose screening applications). Currently, some manufacturers provide a $CTDI_{vol}$ value for the CT localizer radiograph, even though the CTDI concept is not applicable to planar projection radiography.

AAPM Task Group 246 and EFOMP recommend that:

1. Reported $CTDI_{vol}$ values from CT localizer radiographs should not be used to estimate patient doses and should particularly not be used to estimate SSDE. Patient dose from CT localizer radiographs, which irradiate the patient using a narrow fan beam, should be estimated by integration of the entrance skin exposure using a phantom and geometry similar to that used in standard radiography dose measurements.

Despite the robustness of the SSDE concept, it still has limits from a patient radiation dosimetry perspective. The SSDE is not well suited for estimating dose from partial organ irradiations, and it does not communicate information on the spatial distribution of dose. Even if organs are fully contained in the primary x-ray beam, the SSDE only provides the average dose to a certain volume or region, since it is based on a spatially weighted average of $CTDI_{100}$ measurements ($CTDI_w$). Peripheral and central organs in the same irradiated region cannot be assumed to receive the same dose due to attenuation, adding uncertainty to patient organ dose estimates based on the SSDE.

Organ dose estimates can be calculated by Monte Carlo methods, which incorporate distinct parameters for CT scanners and computational phantoms that more closely match the patients. As discussed in this report, modeling patients and CT scanners requires significant effort, and the most refined solutions are thus presently found in proprietary software and research initiatives. Accurate input data improve the accuracy obtained from both Monte Carlo methods and the SSDE calculations. Use of actual $CTDI_w$ measurements help make patient organ dose estimates reflect an actual CT scanner and not the typical make and model, which is reflected in the tabulated values supplied by a manufacturer in DICOM. Use of actual measurements may decrease the uncertainty of the radiation output ($CTDI_w$ and $CTDI_{vol}$), and consequently also the uncertainty of organ dose estimates from 40% to 5%.

2. Given the present refinement of methods for estimating patient organ dose, AAPM Task Group 246 and EFOMP recommend that efforts be made to perform uncertainty analysis of the respective methods, and that reports of patient organ dose should be accompanied by documented estimates of the uncertainty.

   Patient organ dose estimates from Monte Carlo methods and the SSDE also share the need of pertinent examination-specific information found in DICOM (both in image header data and the RDSR), particularly to be able to perform automatic computations. While manual computation is certainly possible, it decreases the applicability and limits the possibilities of the clinical medical physicist to perform required tasks in optimization of radiation dose and image quality.

3. In the interest of improving adoption of the SSDE formalism, AAPM Task Group 246 and EFOMP support the additional recommendations of AAPM report 220, which specifically recommends that manufacturers of CT scanners report the WED for reconstructed images, e.g., 5 mm slice thickness, as part of the RDSR.

4. Furthermore, for purposes of Monte Carlo modeling, it is recommended that manufacturers report tube current (mA) both in the longitudinal (e.g., for 5-mm slice thickness) and rotational plane (e.g., every 5 degrees) to improve the gold standard for benchmarking more simple methods of estimating organ dose.

5. AAPM Task Group 246 and EFOMP also recommend that the steps used to benchmark and validate Monte Carlo simulation results be reported together with organ dose estimates, according to publications by AAPM Task Groups 195 and 268.[100,101]

   AAPM Task Group 246 and EFOMP have identified several changes to the presently available DICOM information that will enhance the ability to estimate patient organ dose. Modifications and additions to DICOM procedural information were also noted, which are not immediately relevant for estimating dose, but which have high importance for quality assur-

ance and longitudinal dose monitoring. Further collaboration with MITA, FDA, IEC, manufacturers of CT scanners, and the DICOM community will be crucial to advancing the calculation and reporting of organ dose.

6. AAPM Task Group 246 and EFOMP recommend that a medical physicist should verify CT scanner RDSR information as part of commissioning and acceptance testing. Furthermore, RDSR verification is also advisable following CT scanner software upgrades.
7. Furthermore, familiarity with RDSR information and other DICOM content, as discussed in this report, may be considered as newly added competence requirements for medical physicists involved in optimization of CT examination protocols and image quality assurance.

6. References

1. American Association of Physicists in Medicine. AAPM Position Statement on Radiation Risks from Medical Imaging Procedures (Policy 25-A). American Association of Physicists in Medicine. https://www.aapm.org/org/policies/details.asp?type=PP&id=318. Published 2011. Accessed February 5, 2018.
2. International Electrotechnical Commission. IEC 6060-2-44 Edition 3.2. Medical electrical equipment – Part 2-44: Particular requirements for the basic safety and essential performance of X-ray equipment for computed tomography. Geneva, Switzerland: 2016.
3. American Association of Physicists in Medicine. AAPM Committee Tree: Computed Tomography Subcommittee. American Association of Physicists in Medicine. https://www.aapm.org/org/structure/default.asp?committee_code=CTSC. Published 2004. Accessed February 5, 2018.
4. International Commission on Radiological Protection. (2007) The 2007 Recommendations of the International Commission on Radiological Protection. *Ann. ICRP.* 37:1–332.
5. Jucius, R. A. and G. X. Kambic. (1977). Radiation dosimetry in computed tomography. *Appl. Opt. Instrum. Eng. Med. Phys.* 127:286–95.
6. Shope, T. B., R. M. Gagne, and G. C. Johnson. (1991). A method for describing the doses delivered by transmission x-ray computed tomography. *Med. Phys.* 8:488–95.
7. ICRU Report No. 87: Radiation dose and image-quality assessment in computed tomography. (2012.) *J. ICRU* 12(1):1–149.
8. American Association of Physicists in Medicine. Report of AAPM Task Group 96. The measurement, reporting, and management of radiation dose in CT. American Association of Physicists in Medicine. https://www.aapm.org/pubs/reports/RPT_96.pdf. Published 2008. Accessed February 6, 2018.
9. McCollough, C.H., S. Leng, L. Yu, D. D. Cody, J. M. Boone, and M. F. McNitt-Gray. (2011). CT dose index and patient dose: they are not the same thing. *Radiology* 259(2):311–16.
10. McNitt-Gray, M. F. (2002). AAPM/RSNA Physics Tutorial for Residents: Topics in CT. Radiation dose in CT. *Radiographics* 22(6):1541–53.
11. European Commission. EUR 16262 EN: European guidelines on quality criteria for computed tomography. http://www.drs.dk/guidelines/ct/quality/index.htm. Published 2000. Accessed February 19, 2018.
12. American Association of Physicists in Medicine. Report of AAPM Task Group 111. Comprehensive Methodology for the Evaluation of Radiation Dose in X-ray Computed Tomography. A New Measurement Paradigm Based on a Unified Theory for Axial, Helical, Fan-Beam, and Cone-Beam Scanning With or Without Longitudinal Translation of the Patient Table. American Association of Physicists in Medicine. https://www.aapm.org/pubs/reports/RPT_111.pdf. Published 2010. Accessed February 6, 2018.

13. Boone, J. M. (2009). Dose spread functions in computed tomography: a Monte Carlo study. *Med. Phys.* 36(10):4547–54.
14. Bahar Gogani, J., P. Hagglund, and G. Wickman. (2005). Assessment of correlated dose and sensitivity profiles on a multi-slice CT scanner. *Radiat. Prot. Dosim.* 114(1–3):332–36.
15. Wickman, G., B. Johansson, J. Bahar-Gogani, T. Holmstrom, and J. E. Grindborg. (1998). Liquid ionization chambers for absorbed dose measurements in water at low dose rates and intermediate photon energies. *Med. Phys.* 25(6):900–07.
16. Jones, D. G. and P. C. Shrimpton. Report NRPB-R250: Survey of CT practice in the UK Part 3: normalized organ doses calculated using Monte Carlo techniques. National Radiological Protection Board: 1991.
17. Jones, D. G. and B. F. Wall. Report NRPB-R186: Organ doses from medical x-ray examinations calculated using Monte Carlo techniques National Radiological Protection Board: 1985.
18. Mathieu, K. B., M. F. McNitt-Gray, D. Zhang, H. J. Kim, and D. D. Cody. (2010). Precision of dosimetry-related measurements obtained on current multidetector computed tomography scanners. *Med. Phys.* 37(8):4102–09.
19. McCollough, C. H. and F. E. Zink. (1999). Performance evaluation of a multi-slice CT system. *Med. Phys.* 26(11):2223–30.
20. International Atomic Energy Agency. *IAEA Human Health Reports No. 5. Status of Computed Tomography Dosimetry for Wide Cone Beam Scanners.* Vienna, Austria: 2011.
21. Platten, D. J., I. A. Castellano, C. L. Chapple, et al. (2013). Radiation dosimetry for wide-beam CT scanners: recommendations of a working party of the Institute of Physics and Engineering in Medicine. *Br. J. Radiol.* 86(1027):20130089.
22. Bauhs, J. A., T. J. Vrieze, A. N. Primak, M. R. Bruesewitz, and C. H. McCollough. (2008). CT dosimetry: comparison of measurement techniques and devices. *Radiographics* 28(1):245–53.
23. Dixon, R. L. and J. M. Boone. (2014). Stationary table CT dosimetry and anomalous scanner-reported values of CTDIvol. *Med. Phys.* 41(1):011907.
24. Bakalyar, D., E. Angel, J. Boone, et al. Making Proper Use of the ICRU/AAPM CT Dose Phantom: Recommendations and Limitations. Paper presented at: Radiological Society of North America Scientific Assembly and Annual Meeting 2015, Chicago, IL.
25. Christner, J. A., V. A. Zavaletta, C. D. Eusemann, A. I. Walz-Flannigan, and C. H. McCollough. (2010). Dose reduction in helical CT: dynamically adjustable z-axis X-ray beam collimation. *AJR Am. J. Roentgenol.* 194(1):W49–55.
26. Digital Imaging and Communications in Medicine (DICOM). The DICOM Standard. https://www.dicomstandard.org/current/. Accessed February 19, 2018.
27. American Association of Physicists in Medicine. Report of AAPM Task Group 220. Use of Water Equivalent Diameter for calculating patient size and Size-Specific Dose Estimates (SSDE) in CT. American Association of Physicists in Medicine. https://www.aapm.org/pubs/reports/RPT_220.pdf. Published 2012. Accessed February 5, 2018.
28. American Association of Physicists in Medicine. Report of AAPM Task Group 204. Size-Specific Dose Estimates (SSDE) in Pediatric and Adult Body CT Examinations. American Association of Physicists in Medicine. https://www.aapm.org/pubs/reports/RPT_204.pdf. Published 2012. Accessed February 5, 2018.
29. Leng, S., M. Shiung, X. Duan, L. Yu, Y. Zhang, and C. H. McCollough. Size Specific Dose Estimation in Abdominal CT: Impact of Longitudinal Variations in Patient Size. Paper presented at: 55th Annual Meeting & Exhibition of the AAPM 2013, Indianapolis, IN.
30. Bostani, M., K. McMillan, P. Lu, et al. (2015). Attenuation-based size metric for estimating organ dose to patients undergoing tube current modulated CT exams. *Med. Phys.* 42(2):958–68.

31. Khatonabadi, M., H. J. Kim, P. Lu, et al. (2013). The feasibility of a regional CTDIvol to estimate organ dose from tube current modulated CT exams. *Med. Phys.* 40(5):051903.
32. Hardy, A., M. Bostani, C. H. Cagnon, and M. McNitt-Gray. Comparison of Size-Specific Dose Estimate Conversion Factors for Fixed Tube Current and Tube Current Modulated Computed Tomography. Paper presented at: Radiological Society of North America Scientific Assembly and Annual Meeting 2016, Chicago, IL.
33. McMillan, K. Estimating Radiation Dose Metrics for Patients Undergoing Tube Current Modulation CT Scans. University of California, Los Angeles, 2015.
34. McMillan, K., M. Bostani, L. Yu, et al. Size-Specific Effective Dose Estimates in Abdominal and Chest CT Exams Using Either Fixed Tube Current or Tube Current Modulation. Paper presented at: Radiological Society of North America Scientific Assembly and Annual Meeting 2015, Chicago, IL.
35. Wang, J., J. A. Christner, X. Duan, S. Leng, L. Yu, and C. H. McCollough. (2012). Attenuation-based estimation of patient size for the purpose of size specific dose estimation in CT. Part II. Implementation on abdomen and thorax phantoms using cross sectional CT images and scanned projection radiograph images. *Med. Phys.* 39(11):6772–78.
36. McMillan, K., M. Bostani, C. H. Cagnon, et al. (2017). Estimating patient dose from CT exams that use automatic exposure control: Development and validation of methods to accurately estimate tube current values. *Med. Phys.* 44(8):4262–75.
37. Moore, B. M., S. L. Brady, A. E. Mirro, and R. A. Kaufman. (2014). Size-specific dose estimate (SSDE) provides a simple method to calculate organ dose for pediatric CT examinations. *Med. Phys.* 41(7):071917.
38. McMillan, K., M. Bostani, C. Cagnon, M. Zankl, A. R. Sepahdari, and M. McNitt-Gray. (2014). Size-specific, scanner-independent organ dose estimates in contiguous axial and helical head CT examinations. *Med. Phys.* 41(12):121909.
39. Hardy, A. J., M. Bostani, A. M. Hernandez, et al. (2019). Estimating a size-specific dose for helical head CT examinations using Monte Carlo simulation methods. *Med. Phys.* 46(2):902–12.
40. Petoussi-Henss, N., M. Zanki, U. Fill, and D. Regulla. (2002). The GSF family of voxel phantoms. *Phys. Med. Biol.* 47(1):89–106.
41. Bostani, M., K. McMillan, J. J. DeMarco, C. H. Cagnon, and M. F. McNitt-Gray. (2014). Validation of a Monte Carlo model used for simulating tube current modulation in computed tomography over a wide range of phantom conditions/challenges. *Med. Phys.* 41(11):112101.
42. Bostani, M., J. W. Mueller, K. McMillan, et al. (2015). Accuracy of Monte Carlo simulations compared to in-vivo MDCT dosimetry. *Med. Phys.* 42(2):1080–86.
43. Khatonabadi, M., D. Zhang, K. Mathieu, et al. (2012). A comparison of methods to estimate organ doses in CT when utilizing approximations to the tube current modulation function. *Med. Phys.* 39(8):5212–28.
44. McCollough, C. H., J. Wang, and L. L. Berland. (2011). Bismuth shields for CT dose reduction: do they help or hurt? *J. Am. Coll. Radiol.* 8(12):878–79.
45. Wang, J., X. Duan, J. A. Christner, S. Leng, K. L. Grant, and C. H. McCollough. (2012). Bismuth shielding, organ-based tube current modulation, and global reduction of tube current for dose reduction to the eye at head CT. *Radiology* 262(1):191–98.
46. Wang, J., X. Duan, J. A. Christner, S. Leng, L. Yu, and C. H. McCollough. (2011). Radiation dose reduction to the breast in thoracic CT: comparison of bismuth shielding, organ-based tube current modulation, and use of a globally decreased tube current. *Med. Phys.* 38(11):6084–92.
47. Li, X., K. Yang, and B. Liu. (2016). A study of the midpoint dose to CTDIvol ratio: Implications for CT dose evaluation. *Med. Phys.* 43(11):5878.

48. Sinclair, L., A. Mench, T. Griglock, S. Bidari, and M. Arreola. Validation of Size-Specific Dose Estimates (SSDE) in Body CT Studies with Directly Measured Organ Doses in Adult Female Cadaveric Subjects. Paper presented at: 55th Annual Meeting of the American Association of Physicists in Medicine 2013, Indianapolis, IN.
49. Boone, J. M. (1999). Glandular breast dose for monoenergetic and high-energy X-ray beams: Monte Carlo assessment. *Radiology* 213(1):23–37.
50. Boone, J. M. (2009). Normalized glandular dose (DgN) coefficients for arbitrary X-ray spectra in mammography: computer-fit values of Monte Carlo derived data. *Med. Phys.* 29(5):869–75.
51. Boone, J. M., A. L. Kwan, J. A. Seibert, N. Shah, K. K. Lindfors, and T. R. Nelson. (2005). Technique factors and their relationship to radiation dose in pendant geometry breast CT. *Med. Phys*. 32(12):3767–76.
52. Dance, D. R. (1990). Monte Carlo calculation of conversion factors for the estimation of mean glandular breast dose. *Phys. Med. Biol.* 35(9):1211–19.
53. Dance, D. R., C. L. Skinner, K. C. Young, J. R. Beckett, and C. J. Kotre. (2000). Additional factors for the estimation of mean glandular breast dose using the UK mammography dosimetry protocol. *Phys. Med. Biol.* 45(11):3225–40.
54. Dance, D. R., K. C. Young, and R. E. van Engen. (2009). Further factors for the estimation of mean glandular dose using the United Kingdom, European and IAEA breast dosimetry protocols. *Phys. Med. Biol.* 54(14):4361–72.
55. Dance, D. R., K. C. Young, and R. E. van Engen. (2011). Estimation of mean glandular dose for breast tomosynthesis: factors for use with the UK, European and IAEA breast dosimetry protocols. *Phys. Med. Biol.* 56(2):453–71.
56. Hammerstein, G. R., D. W. Miller, D. R. White, M. E. Masterson, H. Q. Woodard, and J. S. Laughlin. (1979). Absorbed radiation dose in mammography. *Radiology* 130(2):485–91.
57. Sechopoulos, I. and C. J. D'Orsi. (2008). Glandular radiation dose in tomosynthesis of the breast using tungsten targets. *J. Appl. Clin. Med. Phys.* 9(4):2887.
58. Sechopoulos, I., S. S. Feng, and C. J. D'Orsi. (2010). Dosimetric characterization of a dedicated breast computed tomography clinical prototype. *Med. Phys.* 37(8):4110–20.
59. Sechopoulos, I., S. Suryanarayanan, S. Vedantham, C. D'Orsi, and A. Karellas. (2007). Computation of the glandular radiation dose in digital tomosynthesis of the breast. *Med. Phys.* 34(1):221–32.
60. Khatonabadi, M., D. Zhang, J. Yang, J. J. Demarco, C. C. Cagnon, and M. McNitt-Gray. (2012). The relationship between organ dose and patient size in tube current modulated adult thoracic CT scans. *Proc. SPIE* 8313:83131Q.
61. Wang, J., X. Duan, J. A. Christner, S. Leng, L. Yu, and C. H. McCollough. (2012). Attenuation-based estimation of patient size for the purpose of size specific dose estimation in CT. Part I. Development and validation of methods using the CT image. *Med. Phys.* 39(11):6764–71.
62. Mueller, J. W., D. J. Vining, A. K. Jones, et al. (2014). In vivo CT dosimetry during CT colonography. *AJR Am. J. Roentgenol.* 202(4):703–10.
63. Angel, E., C. V. Wellnitz, M. M. Goodsitt, et al. (2008). Radiation dose to the fetus for pregnant patients undergoing multidetector CT imaging: Monte Carlo simulations estimating fetal dose for a range of gestational age and patient size. *Radiology* 249(1):220–27.
64. Huda, W., D. Magill, and M. V. Spampinato. (2011). Technical note: estimating absorbed doses to the thyroid in CT. *Med. Phys.* 38(6):3108–13.
65. Huda, W., M. V. Spampinato, S. V. Tipnis, and D. Magill. (2013). Computation of thyroid doses and carcinogenic radiation risks to patients undergoing neck CT examinations. *Radiat. Prot. Dosimetry* 156(4):436–44.

66. Zhang, D., C. H. Cagnon, J. P. Villablanca, et al. (2012). Peak skin and eye lens radiation dose from brain perfusion CT based on Monte Carlo simulation. *AJR Am. J. Roentgenol.* 198(2):412–17.
67. Lopez-Rendon, X., A. Stratis, W. Coudyzer, W. Develter, H. Bosmans, and F. Zanca. Dose to the Eye Lens and Skin in CT Perfusion Exams. Paper presented at: 102nd Radiological Society of North America Scientific Assembly and Annual Meeting 2016, Chicago, IL.
68. Zhang, D., C. H. Cagnon, J. P. Villablanca, et al. (2013). Estimating peak skin and eye lens dose from neuroperfusion examinations: use of Monte Carlo based simulations and comparisons to CTDIvol, AAPM Report No. 111, and ImPACT dosimetry tool values. *Med. Phys.* 40(9):091901.
69. U.S. Food and Drug Administration. Radiation Dose Quality Assurance: Questions and Answers. https://www.fda.gov/Radiation-EmittingProducts/RadiationSafety/RadiationDoseReduction/ucm232550.htm. Updated 12/2/2017. Accessed February 7, 2018.
70. de las Heras, H., R. Minniti, S. Wilson, et al. (2013). Experimental estimates of peak skin dose and its relationship to the CT dose index using the CTDI head phantom. *Radiat. Prot. Dosimetry* 157(4):536–42.
71. Leng, S., T. Vrieze, L. Yu, and C. McCollough. Skin Dose Estimation from CT Perfusion Studies: Influence of Patient Size, Beam Collimation and Scanner Type. Paper presented at: 96th Scientific Assembly and Annual Meeting of the Radiological Society of North America 2010, Chicago, IL.
72. Dixon, R. L. (2003). A new look at CT dose measurement: beyond CTDI. *Med. Phys.* 30(6):1272–80.
73. Dixon, R. L. and J. M. Boone. (2011). Analytical equations for CT dose profiles derived using a scatter kernel of Monte Carlo parentage with broad applicability to CT dosimetry problems. *Med. Phys.* 38(7):4251–64.
74. Dixon, R. L., J. M. Boone, and R. A. Kraft. (2014). Dose equations for shift-variant CT acquisition modes using variable pitch, tube current, and aperture, and the meaning of their associated CTDI(vol). *Med. Phys.* 41(11):111906.
75. Tian, X., W. P. Segars, R. L. Dixon, and E. Samei. (2016). Convolution-based estimation of organ dose in tube current modulated CT. *Phys. Med. Biol.* 61(10):3935–54.
76. Segars, W. P., J. Bond, J. Frush, et al. (2013). Population of anatomically variable 4D XCAT adult phantoms for imaging research and optimization. *Med. Phys.* 40(4):043701.
77. Li, X., W. P. Segars, and E. Samei. (2014). The impact on CT dose of the variability in tube current modulation technology: a theoretical investigation. *Phys. Med. Biol.* 59(16):4525–48.
78. Jansen, J. T. and P. C. Shrimpton. (2011). Calculation of Normalised Organ and Effective Doses to Adult Reference Computational Phantoms from Contemporary Computed Tomography Scanners. *Prog. Nucl. Sci. Technol.* 2:165–71.
79. Jansen, J. T. and P. C. Shrimpton. Normalized doses for various reference patients and a range of computed tomography scanners. Paper presented at: Proceedings of CP 2013: 4th International Workshop on Computational Phantoms for Radiation Protection, Imaging and Radiotherapy 2013.
80. Li, X., E. Samei, T. Yoshizumi, J. G. Colsher, R. P. Jones, and D. P. Frush. (2007). Experimental benchmarking of a Monte Carlo dose simulation code for pediatric CT. *Proc. SPIE* 6510:65102A.
81. Li, X., D. Zhang, and B. Liu. (2012). Estimation of the weighted CTDI(infinity) for multislice CT examinations. *Med. Phys.* 39(2):901–05.
82. Oono, T., F. Araki, S. Tsuduki, and K. Kawasaki. (2014). Monte Carlo calculation of patient organ doses from computed tomography. *Radiol. Phys. Technol.* 7(1):176–82.

83. van Straten, M., P. Deak, P. C. Shrimpton, and W. A. Kalender. (2009). The effect of angular and longitudinal tube current modulations on the estimation of organ and effective doses in x-ray computed tomography. *Med. Phys.* 36(11):4881–89.
84. Zhang, Y., X. Li, W. P. Segars, and E. Samei. (2013). Comparative dosimetry of radiography, tomosynthesis, and CT for chest imaging across 59 adult patients. *Proc. SPIE* 8668:866844.
85. Stepusin, E. J., D. J. Long, K. R. Ficarrotta, D. E. Hintenlang, and W. E. Bolch. (2017). Physical validation of a Monte Carlo-based, phantom-derived approach to computed tomography organ dosimetry under tube current modulation. *Med. Phys.* 44(10):5423–32.
86. Stepusin, E. J., D. J. Long, E. L. Marshall, and W. E. Bolch. (2017). Assessment of different patient-to-phantom matching criteria applied in Monte Carlo-based computed tomography dosimetry. *Med. Phys.* 44(10):5498–508.
87. International Commission on Radiological Protection. (2010). Publication No. 116. Conversion coefficients for radiological protection quantities for external radiation exposures. *Ann. ICRP* 40:1–257.
88. Johnson, P. B., A. A. Bahadori, K. F. Eckerman, C. Lee, and W. E. Bolch. (2011). Response functions for computing absorbed dose to skeletal tissues from photon irradiation—an update. *Phys. Med. Biol.* 56(8):2347–65.
89. International Commission on Radiological Protection. (1975). Publication No. 23. Report of the Task Group on Reference Man. *Ann. ICRP* 23:1–480.
90. International Commission on Radiological Protection. (2002). Publication No. 89. Basic Anatomical and Physiological Data for Use in Radiological Protection Reference Values. *Ann. ICRP* 32(3–4):1–277.
91. Turner, A. C., D. Zhang, H. J. Kim, et al. (2009). A method to generate equivalent energy spectra and filtration models based on measurement for multidetector CT Monte Carlo dosimetry simulations. *Med. Phys.* 36(6):2154–64.
92. Caon, M., G. Bibbo, and J. Pattison. (1997). A comparison of radiation dose measured in CT dosimetry phantoms with calculations using EGS4 and voxel-based computational models. *Phys. Med. Biol.* 42(1):219–29.
93. Jarry, G., J. J. DeMarco, U. Beifuss, C. H. Cagnon, and M. F. McNitt-Gray. (2003). A Monte Carlo-based method to estimate radiation dose from spiral CT: from phantom testing to patient-specific models. *Phys. Med. Biol.* 48(16):2645–63.
94. Zhang, D., A. S. Savandi, J. J. Demarco, et al. (2009). Variability of surface and center position radiation dose in MDCT: Monte Carlo simulations using CTDI and anthropomorphic phantoms. *Med. Phys.* 36(3):1025–38.
95. Zhang, D., M. Zankl, J. J. DeMarco, et al. (2009). Reducing radiation dose to selected organs by selecting the tube start angle in MDCT helical scans: a Monte Carlo based study. *Med. Phys.* 36(12):5654–64.
96. Angel, E., N. Yaghmai, C. M. Jude, et al. (2009). Dose to radiosensitive organs during routine chest CT: effects of tube current modulation. *AJR Am. J. Roentgenol.* 193(5):1340–45.
97. Angel, E., N. Yaghmai, C. M. Jude, et al. (2009). Monte Carlo simulations to assess the effects of tube current modulation on breast dose for multidetector CT. *Phys. Med. Biol*. 54(3):497–512.
98. Jansen, J. T. and P. C. Shrimpton. Calculation of Normalized Organ Doses for Pediatric Patients Undergoing CT Examinations on Four Types of CT Scanner. Paper presented at: World Congress on Medical Physics and Biomedical Engineering 2009, Munich, Germany.
99. Kalender, W. A., N. Saltybaeva, D. Kolditz, M. Hupfer, M. Beister, and B. Schmidt. (2014). Generating and using patient-specific whole-body models for organ dose estimates in CT with increased accuracy: feasibility and validation. *Phys. Med.* 30(8):925–33.

100. American Association of Physicists in Medicine. Electronic Resources of the TG 195 Report. Monte Carlo Reference Data Sets for Imaging Research. American Association of Physicists in Medicine. https://www.aapm.org/pubs/reports/report195.asp. Accessed February 7, 2018.
101. Sechopoulos, I., D. W. O. Rogers, M. Bazalova-Carter, et al. (2018). RECORDS: improved Reporting of montE CarlO RaDiation transport Studies. *Int. J. Radiat. Oncol. Biol. Phys.* 101(4):792–93.
102. Martin, C. J. (2007). Effective dose: how should it be applied to medical exposures? *Br. J. Radiol.* 80(956):639–47.
103. Martin, C. J. (2008). The application of effective dose to medical exposures. *Radiat. Prot. Dosimetry* 128(1):1–4.
104. Joint Committee for Guides in Metrology (JCGM). JCGM 100:2008. Evaluation of measurement data - Guide to the expression of uncertainty in measurement https://www.bipm.org/utils/common/documents/jcgm/JCGM_100_2008_E.pdf. Published 2008. Accessed February 19, 2018.
105. Zanca, F., A. Jacobs, W. Crijns, and W. De Wever. (2014). Comparison of measured and estimated maximum skin doses during CT fluoroscopy lung biopsies. *Med. Phys.* 41(7):073901.
106. Ding, A., M. M. Mille, T. Liu, P. F. Caracappa, and X. G. Xu. (2012). Extension of RPI-adult male and female computational phantoms to obese patients and a Monte Carlo study of the effect on CT imaging dose. *Phys. Med. Biol.* 57(9):2441–59.
107. Geyer, A. M., S. O'Reilly, C. Lee, D. J. Long, and W. E. Bolch. (2014). The UF/NCI family of hybrid computational phantoms representing the current US population of male and female children, adolescents, and adults--application to CT dosimetry. *Phys. Med. Biol.* 59(18):5225–42.
108. Samei, E., X. Tian, and W. P. Segars. (2014). Determining organ dose: the holy grail. *Pediatr. Radiol.* 44 Suppl 3:460–67.
109. Schlattl, H., M. Zankl, J. Becker, and C. Hoeschen. (2010) Dose conversion coefficients for CT examinations of adults with automatic tube current modulation. *Phys. Med. Biol.* 55(20):6243–61.
110. Tian, X., X. Li, W. P. Segars, D. P. Frush, E. K. Paulson, and E. Samei. (2013). Dose coefficients in pediatric and adult abdominopelvic CT based on 100 patient models. *Phys. Med. Biol.* 58(24):8755–68.
111. Turner, A. C., D. Zhang, M. Khatonabadi, et al. (2011). The feasibility of patient size-corrected, scanner-independent organ dose estimates for abdominal CT exams. *Med. Phys.* 38(2):820–29.
112. Zhang, Y., X. Li, W. P. Segars, and E. Samei. (2012). Organ doses, effective doses, and risk indices in adult CT: comparison of four types of reference phantoms across different examination protocols. *Med. Phys.* 39(6):3404–23.
113. Liu, H., J. Gu, P. F. Caracappa, and X. G. Xu. (2010). Comparison of two types of adult phantoms in terms of organ doses from diagnostic CT procedures. *Phys. Med. Biol.* 55(5):1441–51.
114. Kallman, H. E., R. Holmberg, J. Andersson, L. Kull, E. Traneus, and A. Ahnesjo. (2016). Source modeling for Monte Carlo dose calculation of CT examinations with a radiotherapy treatment planning system. *Med. Phys.* 43(11):6118.
115. Sahbaee, P., W. P. Segars, and E. Samei. Multi-phase CT: Impact of Contrast Medium Propagation on Radiation Dose across a Population of Patient Models. Paper presented at: Radiological Society of North America 2014 Scientific Assembly and Annual Meeting 2014, Chicago, IL.
116. Tran, H., C. Lee, V. Derderian, L. Folio, and E. Jones. Estimating the Role of Iodinated IV Contrast Media in Organ Radiation Dose: Effects of Vascular Phase and Tube Voltage in Multiphase Body CT. Paper presented at: Radiological Society of North America 2014 Scientific Assembly and Annual Meeting 2014, Chicago, IL.

Appendix:

DICOM—Present and Future for Dosimetry and Estimating Organ Dose

Determination of dose estimates, with associated quality assurance efforts, are now an established informatics endeavor, with radiation dose being fully represented as part of the medical imaging electronic environment.[1] This is currently possible with the use of the RDSR, which compiles patient and examination data, technical, geometric, and dosimetric data for each radiation procedure, plus total dose data for the complete procedure. This DICOM object is gaining wide availability for CT. DICOM is the set of standards managed by the National Electrical Manufacturer's Association (NEMA) and is the key method of transferring medical image data. The continuing aim of the DICOM Standard is to achieve a higher level of compatibility between manufacturers and systems for important information content, thereby enabling an enhanced quality of service with improved workflow efficiency between and among imaging systems and other information systems in healthcare environments worldwide.[2–9]

One of the components of the Medical Imaging and Technology Alliance (MITA) standard XR-29 known as MITA Smart Dose is that the CT scanner must be capable of generating a DICOM RDSR.[10] Each manufacturer has set up a vendor certification web portal on the MITA Smart Dose website (http://www.medicalimaging.org/policy-and-positions/mita-smart-dose/). For CT scanners in the United States, compliance with all components of MITA XR-29 was required for full reimbursement of outpatient scans by the Center for Medicare and Medicaid Systems (CMS). Without compliance (effective Jan. 1, 2016), CMS reimbursement is reduced by 5% for outpatient scans in 2016 and by 15% in 2017. Note that compliance with XR-29 is established based on CT scanner capabilities, not on usage. When used appropriately, these features improve the safety of CT scans for the patients and can improve the image quality.

At a high level, radiation dose and related information may be found in three locations: the DICOM tags associated with the produced images' header data, a CT Dose Data Page (known by other names, including the Patient Protocol page, Patient Dose page, etc.), and more recently the RDSR.[11] Quality assurance dose-related information is found in the RDSR, but it also includes DICOM data from the Study, Series, and even Image level tags.

Specifically related to the CT radiation dose, DICOM has a CT Exposure Functional Group with attributes dedicated to capture the CT radiation dose. Examples of existing DICOM attributes in images relating to CT irradiation are listed in Table 2. However, most of these DICOM attributes are "optional" in the DICOM Standard and may not be populated by all CT manufacturers, or some manufacturers may have implemented this information in private tags. Other important parameters useful for patient dose estimates, such as anatomy location, are currently not available in DICOM.

A.1 CT Radiation Dose Reporting from DICOM Objects

This section describes the DICOM content from two different sources, the Dose Data Page and DICOM image header data.

A.1.1 The Dose Data Page

CT manufacturers initially provided a summary of dose information in a Dose Data Page several years prior to the introduction of the DICOM RDSR. The Dose Data Page is an image of text information, automatically created and saved as an image (Secondary Capture), with or without associated dose information in the DICOM image headers. Since manufacturers introduced the Dose Data Page at dif-

ferent times, clinical scanners have different degrees of compliance with optional fields and even required fields. Therefore, the availability of CT dose-related information is totally dependent on the scanner model and the software version currently installed.

For legacy scanners (defined in this context as those devices having only the Dose Data Page), the dose information may only be available from the screen capture once the examination is completed. The Dose Data Page may be sent to the PACS (picture archiving and communication system) as one of the scan series and archived in the image database. The Dose Data Page lists all imaging scan series performed in the examination (even if those image series are not sent to the PACS), and it always includes the $CTDI_{vol}$ and DLP information for each scan series.

To extract the CT radiation dose-related information directly from Dose Data Page images, Optical Character Recognition (OCR) software can be used to read the numerical values of $CTDI_{vol}$ or DLP. [12]

A.1.2 DICOM Image Header Data

CT manufacturers support the use of DICOM standards and have populated the radiation dose-related attributes at the series and image level. This information may be electronically extracted from DICOM image header information using readily available DICOM software. However, there are some fundamental limitations to the dose extraction using image-based DICOM tags. For example, two image sets reconstructed with different image thickness could be generated from the same scan series, therefore the radiation dose parameter extracted from one series is actually duplicated by the other series. DICOM images have an attribute that specifies 'Image Type' (0008,0008). Images that are created from source data are designated *original.* These original images were created by an x-ray irradiation in CT, and differ from those that are *derived* from the *original* data, which are called reprocessed images, e.g., with a different reconstructed image thickness. However, if the CT creates an image series with another reconstruction kernel, these images would also be designated as *original.* If using the image header data only, this second series could be interpreted as an added dose if the Image Type tag is used to differentiate irradiation events. Furthermore, it is possible that the irradiation took place, but the resulting images were not stored on the scanner or sent to the PACS by the operator. Such events would be captured on the Dose Data Page, but it is difficult to automatically associate reconstructed image series with irradiation events.

Since 2008, RDSR has been considered the preferred method for storing and extracting radiation dose related information. The RDSR is discussed in the following sections. RDSR is one member of a more extensive DICOM Structured Report family. RDSR is based on templates to "store" information from different functional groups, such as the CT Exposure Functional Group and CT Acquisition Details Group.

A.2 Radiation Dose Structured Report (RDSR)—The DICOM Object

An RDSR object is structured as a composite object (combination of various information entities), similar to objects in DICOM images. An RDSR encompasses information to relate the object to the right patient, the right examination, and to uniquely identify information generated during the examination. An RDSR object is identified by its DICOM SOP Class identifier "1.2.840.10008.5.1.4.1.1.88.67" and a unique DICOM Instance identifier (UID). An RDSR object is like an image, with the major difference that it does not contain pixel data; instead it contains structured information organized in a "content tree." Current PACS solutions rarely have an RDSR reader, and some legacy PACS cannot even store the RDSR. Use of legacy scanners requires configuration of the CT scanner with a dedicated DICOM storage node to receive Dose Data Pages. A custom DICOM storage can be created for this purpose, or radiation exposure management software can be used. In

principle for CT procedures, the contents can be divided into three parts: (1) DICOM header, (2) dose accumulation container, and (3) container holding the information for each irradiation event. Containers are embedded in a root template container called "X-ray Radiation Dose Report." Together, they form the content tree. The basic module composition of the RDSR is described in PS3.3 Information Object Definitions in section A.35.8 "X-ray Radiation Dose SR Information Object Definition (IOD)".[13]

A.2.1 DICOM Structured Report Templates

A Template Identifier (TID) uniquely specifies a Structured Report *Template* that contains the structure and the rules on filling in the content tree for a specific report. In DICOM, the TID is described in PS3.16 Content Mapping Resource.[14] The top-level template for the CT RDSR is TID 10011 CT Radiation Dose. All TIDs have a simple structure, similar to a table with each line, or row, specifying one content item of the RDSR. Templates are ordered in hierarchical structure and are used to group related content or for repetition (e.g., "CT Irradiation Event Data" for irradiation event-related content, repeated one to many times as a number of acquisitions or CT series are performed). For example, when a physician steps on the pedal for CT Fluoroscopy 34 times, 34 irradiation events are captured, and this occurs for all activation of radiation, including the CT localizer radiograph(s). The present CT RDSR template structure is shown in Figure A1.[12]

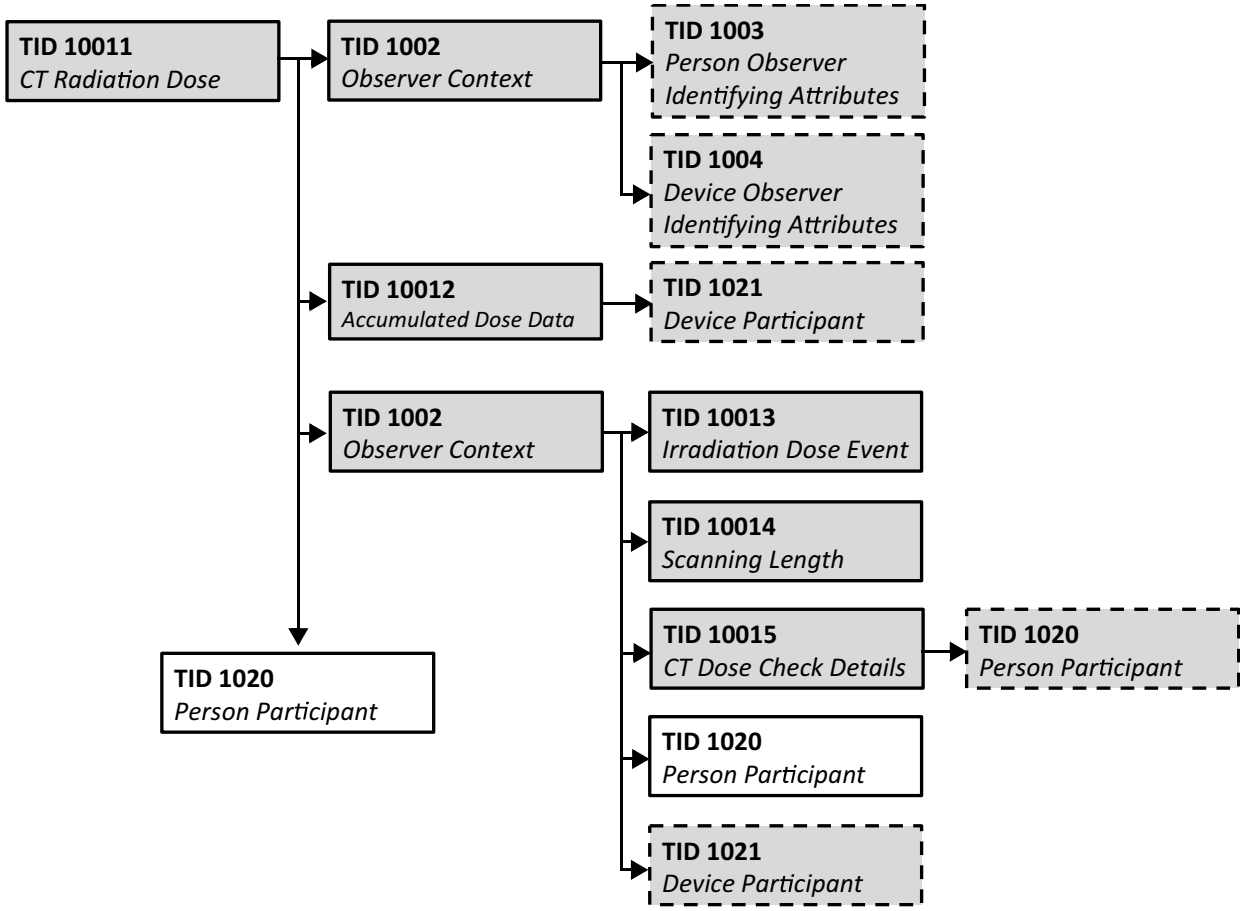

Figure A1. Schema of TIDs used in the CT RDSR.[12]

A.2.2 The Patient RDSR

The RDSR content discussed above is limited to information about the irradiation system or information the system can determine, e.g., radiation output, geometry, x-ray source, detector system, etc. This content is missing pertinent information about the patient that can be used to estimate organ dose. To address this deficiency, the Patient RDSR (P-RDSR) has been added to the DICOM standard. The P-RDSR includes four TIDs, 10031 through 10034, which are detailed below.

TID 10031 Radiation Dose Estimate

This contains the dose information for all organs that were included in the dose estimation. Dose estimation to the whole body or a phantom are possible options that may be used in place of an organ to allow for simple estimations or quality control measurements. Only absorbed dose and equivalent dose are allowed values to be included in the P-RDSR, and a single value for each organ is required. The type of metric this value represents (e.g., maximum, minimum, mean, etc.) is required. There is also an option to include an estimate of the uncertainty in the values if known.

TID 10032 Radiation Dose Estimate Representation

This allows the dose to be stored as a separate DICOM IOD to better visualize the distribution of dose in the patient. Some examples of the representation are as a surface segmentation IOD for skin dose maps, or storing a point cloud of individual dose estimations within a patient for use in more advanced dosimetry.

TID 10033 Radiation Dose Estimate Methodology

This contains the information used in the dose estimation method. The first item to note is that an RDSR that stores the radiation technique factors and output is required. If the modality does not provide an RDSR, one that includes the assumed values must be created. This was done so the P-RDSR did not need to repeat the values already stored in the RDSR. The P-RDSR also provides the ability to list the values within the RDSR that were used in the dose estimation. This is needed if the dose estimation excluded some exposures, e.g., scout/localizer or setup exposures. TID 10033 also includes the patient demographics used by the method (e.g., sex, age, weight, and height). These are only the values used in the method, and need not be the actual patient demographics. This was included to allow storage of the actual values used by the method that may be needed for unique patient habitus, etc. The TID also includes the type of model used to represent the patient (e.g., simple geometric, anthropomorphic, or actual patient segmentation models). The model can also be stored as a separate DICOM IOD, similar to the dose representation. It is hoped that this may promote the development of radiation transport and dosimetry models to be stored as DICOM IOD for standard storage and use. The registration of the patient model to the RDSR from the modality is required. Because the current RDSR does not include a frame of reference, the registration may be a simple visual registration, or it can use fiducial markers or the frame of reference from the images produced to accomplish the registration.

TID 10034 Radiation Dose Estimate Parameters

This is used to store any method-specific parameters used in the estimation. A listing of the parameters that may be included are specified in the DICOM Standard, and the values and units for each must be provided.

A.3 Using the DICOM RDSR

A.3.1 RDSR Reader

A CT RDSR is organized as a “content tree” with at least three major components: DICOM header information, a container for CT accumulated dose data (based on TID 10012), and another container

- :CONTAINER:X-Ray Radiation Dose Report [SEPARATE] (DCMR, 10011)
- HAS CONCEPT MOD: CODE: Procedure reported = Computed Tomography X-ray
  - *HAS OBS CONTEXT: CODE: Observer Type = Device*
  - *HAS OBS CONTEXT: UIDREF: Device Observer UID = 1.3.46.670589.33.1.2200303521616*
  - *HAS OBS CONTEXT: TEXT: Device Observer Name = MACHINE4019*
  - *HAS OBS CONTEXT: TEXT: Device Observer Manufacturer = Philips*
  - *HAS OBS CONTEXT: TEXT: Device Observer Model Name = Ingenuity CT*
  - *HAS OBS CONTEXT: TEXT: Device Observer Serial Number =1234*
  - *HAS OBS CONTEXT: TEXT: Device Observer Physical Location During Observation = PMSTL*
  - *HAS OBS CONTEXT: DATETIME: Start of X-Ray Irradiation = 20120717090534.295*
  - *HAS OBS CONTEXT: DATETIME: End of X-Ray Irradiation = 20120717090550.572*
- HAS OBS CONTEXT: CODE: Scope of Accumulation = Study
- CONTAINS: CONTAINER: CT Accumulated Dose Data [SEPARATE]
  - CONTAINS: NUM: Total Number of Irradiation Events = 1 events
  - CONTAINS: NUM: CT Dose Length Product Total = 4030.6 mGy.cm
- CONTAINS: CONTAINER: CT Acquisition [SEPARATE]
  - CONTAINS: TEXT: Acquisition Protocol = Brain Helical /Head
  - CONTAINS: CODE: Target Region = Brain
  - CONTAINS: CODE: CT Acquisition Type = Spiral Acquisition
  - CONTAINS: CODE: Procedure Context = Diagnostic radiography with contrast media
  - CONTAINS: UIDREF: Irradiation Event UID = 1.3.46.670589.33.1.37611252433939500353.3009441819409284647 9

Figure A.2. CT RDSR tree-like structure with containers based on TID 10012 and 10013.

for individual CT irradiation dose event (based on TID 10013). CT RDSR itself is an encoded tree-like representation "layered" on top of traditional DICOM header data (see Figure A2).

An RDSR reader (or viewer) is typically necessary to parse these datasets into a human-readable format. However, data can be extracted from RDSRs in a number of ways:

- Command line tools exist that can present the entire object as text in the form of a DICOM dump. These tools are very useful for troubleshooting and quick checks, but the hierarchy, repetition, and volume of information makes them unsuitable for general clinical use.
- Some RDSR readers can present the content in a formatted way, as shown in Figure A3. However, in order to avoid these reports being too long and unwieldy, the authors of the software may have selected the fields that they consider to be pertinent. The reports present only the preselected types of data.
- Some software products can compile a collection of RDSRs and present selected data in a spreadsheet in per study/per event detail and summarize the data over all the studies. Similar to text reports, the spreadsheet does not present all data.
- Radiation dose management software configures RDSRs into a database. The data can be viewed and manipulated, commonly in a web browser, and usually can be exported to a spreadsheet. The extent of the stored data and user access varies with the software.

All aforementioned software can be obtained as open source and from commercial providers.[15] The NEMA DICOM Working Group 28 acts as a liaison body to facilitate including data relevant to the medical physics community in the DICOM standard used by manufacturers of x-ray equipment and software providers.

X-Ray Radiation Dose Report

Patient ID:	**Name:**
Birth date:	**Age:**
Sex:	**Ethnic group:**
Exam Date:	**Exam No.:**
Accession Number:	**Content Date:**
Weight:	**Body Surface Area:**
Height:	**Body Mass Index:**
Cardiologist:	**Referring Physician:**
Completion flag: COMPLETE	**Verification flag:** UNVERIFIED

Procedure reported	Computed Tomography X-Ray
Has Intent	Diagnostic Intent
Observer Type	Device
Device Observer UID	73657
Device Observer Name	PX_CT02RAA031791
Device Observer Manufacturer	SIEMENS
Device Observer Model Name	SOMATOM Definition Flash
Device Observer Serial Number	73657
Device Observer Physical Location During Observation	Mayo Clinic PXMH CT02_1665
Start of X-Ray Irradiation	2013-07-24, 09:40:10.010988
End of X-Ray Irradiation	2013-07-24, 09:53:48.372994
Scope of Accumulation	Study
Study Instance UID	1.2.124.113532.172.16.49.225.20130724.91741.2035726
CT Accumulated Dose Data	
Total Number of Irradiation Events	8.0 {events}
CT Dose Length Product	5,346.0 mGycm
CT Acquisition	
Acquisition Protocol	Topogram
Target Region	Head
CT Acquisition Type	Constant Angle Acquisition
Procedure Context	CT without contrast
Irradiation Event UID	1.3.12.2.1107.5.1.4.73657.30000013072404121171200000040
CT Acquisition Parameters	
Exposure Time	4.3 s
Scanning Length	418.0 mm
Nominal Single Collimation Width	0.6 mm
Number of X-Ray Sources	1.0 {X-Ray sources}

Figure A.3. An example of the plain text format from a CT RDSR reader.

A.3.2 Verification of the DICOM RDSR

A physicist needs to verify that a CT scanner has the capability of generating a correct RDSR as part of the CT acceptance test, or as part of a software upgrade for RDSR functionality. A healthcare system uses these data as a record of individual patient exposure, and all data should thus be validated. If a permanent RDSR storage solution is not available at the point of acceptance, the RSDR should be exported from the scanner along with the acceptance images, for example by exporting to a travel drive or an external hard drive.

The exported data should be inspected and the accuracy validated using any of the tools in section A.3.1, along with the manufacturer DICOM conformance statement. Technical values such as $CTDI_{vol}$ and DLP should be compared with the displayed acquisition parameters, as well as administrative fields, such as the institution name, scanner details, and protocol names. Since these details are often missing or set to defaults, and some technical parameters such as exposure time have been found to be completely wrong, automated linking of the various identifiers with the necessary variables should be a top priority of software upgrades.

Familiarity with the RDSR and other DICOM content may be considered as a newly added competence requirement for medical physicists involved in optimization and image quality assurance.

Appendix References

1. Wang, J., X. Duan, J. A. Christner, S. Leng, L. Yu, and C. H. McCollough CH. (2012). Attenuation-based estimation of patient size for the purpose of size specific dose estimation in CT. Part I. Development and validation of methods using the CT image. *Med. Phys.* 39(11):6764–71.
2. Digital Imaging and Communications in Medicine (DICOM). Change Proposals (1077, 1114, 1151, 1160, 1201, 1223, 1254). http://www.dicomstandard.org/cps/. Accessed February 15, 2018.
3. O'Donnell, K. Correction Proposal (CP-1077): Add CR report type to Dose SR and relax content conditions. 2012. ftp://medical.nema.org/medical/dicom/final/cp1077_ft3.pdf. Accessed February 15, 2018.
4. Correction Proposal (CP-1114): Correct UCUM multiplication. 2011. ftp://medical.nema.org/medical/dicom/final/cp1114_ft.pdf. Accessed February 15, 2018.
5. Hoehn, H. and H. Solomon H. Correction Proposal (CP-1160): Degree sign in UCUM. 2012. ftp://medical.nema.org/medical/dicom/final/cp1160_ft.pdf. Accessed February 15, 2018.
6. Revet, B. and H. Blendinger. Correction Proposal (CP-1151): Correct condition for "number of pulses" in TID 10003. 2011. ftp://medical.nema.org/medical/dicom/final/cp1151_ft.pdf. Accessed February 15, 2018.
7. Nolte, B. and H. Blendinger. Correction Proposal (CP-1201): Correct calibration factor CI definition (TID 10002). 2013. ftp://medical.nema.org/medical/dicom/final/cp1201_ft.pdf. Accessed February 15, 2018.
8. Revet, B. and H. Blendinger. Correction Proposal (CP-1223): Additional items for dose SR (by IEC PT 61910-1). 2013. ftp://medical.nema.org/medical/dicom/final/cp1223_ft2.pdf. Accessed February 15, 2018.
9. Revet B. and H. Blendinger. Correction Proposal (CP-1254): Correct definition of irradiation duration. 2013. ftp://medical.nema.org/medical/dicom/final/cp1254_ft.pdf. Accessed February 15, 2018.
10. National Electrical Manufacturers Association. NEMA XR 29-2013: Standard Attributes on CT Equipment Related to Dose Optimization and Management. In: The Association of Electrical Equipment and Medical Imaging Manufacturers. 2013.
11. Digital Imaging and Communications in Medicine (DICOM). Supplement 127: CT radiation dose reporting (Dose SR). 2007. ftp://medical.nema.org/medical/dicom/final/sup127_ft.pdf. Accessed February 15, 2018.
12. Clunie, D. Dose Utility Usage. http://www.dclunie.com/pixelmed/software/webstart/DoseUtilityUsage.html. Accessed February 6, 2018.
13. Digital Imaging and Communications in Medicine (DICOM). DICOM PS3.3 2017e – Information object definitions. 2017. http://dicom.nema.org/medical/dicom/current/output/chtml/part03/PS3.3.html. Accessed February 15, 2018.
14. Digital Imaging and Communications in Medicine (DICOM). DICOM PS3.16 2017e – Content mapping resource. 2017. http://dicom.nema.org/medical/dicom/current/output/html/part16.html. Accessed February 15, 2018.
15. McDonagh, E. OpenREM: Free and open source radiation exposure monitoring for the physicist. http://openrem.org/. Accessed February 15, 2018.